

Chapter 2

Light Metal Matrix Composites

Abstract Fundamentals of metal matrix composites are overviewed. The various light metal matrix systems (particularly Al and Mg) and the different types of reinforcements used are mentioned. The various composite production methods are described. Strengthening mechanisms that define the enhancement in properties of composites are discussed. The microstructural and mechanical properties of the composites are summarized. In addition, the several disadvantages encountered in MMCs due to ceramic reinforcement addition are understood from interfacial characteristic/properties.

Keywords Light metal matrix composites • Aluminum and magnesium matrices • Ceramic reinforcements • Liquid-state processing methods • Solid state and semi-solid state processes • Strengthening mechanisms • Microstructural and mechanical properties • Limitations

2.1 Background

For the past few decades, there has been a sharp demand for light weight structural materials, especially in the rapidly growing automotive and aerospace industries. In recent times, alloys of Al, Ti, and Mg have gained importance in such applications because of their unique properties and comparative advantages such as light-weight, good machinability, dimensional stability, and energy efficiency/low power consumption. Despite the fact that Al- and Mg-alloys have several attractive properties, they do not completely satisfy the overall requirements in applications where the components are required to withstand high mechanical/thermal stresses and also under tribological conditions. Their alloys present a noticeable decrease of mechanical properties at relatively low temperatures, less than about 200 °C (Surappa 2003; Friedrich and Mordike 2006) which strongly limits their application for critical components in the automotive and aerospace sectors. Hence, there arises a need to improve their properties so to realize their full potential in commercial applications. A reliable route to realize this objective is to make composites from the light metals/alloys. These are called light metal matrix composites (LMMCs) wherein the light

metal matrix is incorporated with a hard reinforcing phase (typically ceramic or carbon based). In LMMCs, the synergistic effect of ductility and toughness of the metal matrix and the high strength and stiffness of the reinforcement are utilized. The introduction of such reinforcements into the light metal matrices significantly improve the mechanical properties such as hardness, tensile strength, elastic modulus, and yield strength, and also give rise to excellent wear resistance. Further improvement in properties can be achieved by proper heat/thermal treatments. Given these advantages, LMMCs are seen to have enormous potential in diverse industrial/commercial sectors such as automotive, aviation, biomedical, sporting equipments, consumer electronics, etc.

2.2 Characteristics of MMCs

In a metal matrix composite, three important features determine its characteristics: viz., the matrix, the reinforcement, and the matrix/reinforcement interface.

Matrix. Matrix is the continuous phase and its properties are improvised by converting it into a composite with the introduction of an appropriate reinforcement. Selection of the matrix and the reinforcement largely depends upon the end use and the amenability for production. For a long time it was assumed that the only function of the matrix was to hold the reinforcement in position. Over the years, the importance of the function of matrix and its influence on the properties has been well established. The metallic matrix being highly structure-sensitive, as any change in its microstructure (by the incorporation of reinforcement) would alter the overall performance of the composite.

Reinforcement. The reinforcement phase in the metal matrix composite is the secondary phase. Due to its high stiffness and high strength, it is the main load bearing member in the composite. Reinforcements are usually ceramics in the form of fibers/whiskers/particles. The morphology and nature of the reinforcements are very important in controlling the final properties, as their interaction with the matrix would alter the composite microstructure, properties, and performance. Also, given the heat-treatable nature of both Al and Mg matrices, it is quite important to also consider the effect of reinforcement on the precipitation mechanisms. Reinforcements are classified into two major categories—continuous reinforcements and discontinuous reinforcements.

1. *Continuous reinforcements:* Continuous fibers are those filamentary materials whose lengths are greater than 100 μm . They can be either amorphous, single crystalline, or polycrystalline. The properties of various continuous fibers are given in Table 2.1 (Harris 1988). Due to their unidirectional nature, the properties of continuous fiber reinforced composites are anisotropic.
2. *Discontinuous reinforcements:* Short fibers, particles, and whiskers are classified as discontinuous reinforcements. Tables 2.2, 2.3, and 2.4 list the properties

Table 2.1 Properties of various continuous fiber reinforcements (Harris 1988)

Fiber type	Diameter (μm)	Density (g/cm^3)	Modulus (GPa)	UTS (MPa)	Breaking strain (%)
Boron, single fiber, SiC coated	100–150	2.70	400	3,100	0.77
α —Alumina, tow	20	3.95	379	1,380	0.36
γ —Alumina, tow	17	3.25	210	1,800	0.85
Carbon, high modulus, tow	8	1.85	400	2,300	0.58
Carbon, high tension, tow	8	1.75	23	2,800	1.10
SiC, tow	13	2.55	196	2,550	1.00
SiC, single fiber	100–140	3.5	400	2,700	0.68

Table 2.2 Properties of particulate reinforcing materials used in MMCs (Giro et al. 1987)

Material	Normal size used (μm)	Density (g/cm^3)
SiC	15–340	3.2
SiO ₂	40–60	2.3
MgO	40–60	2.7–3.6
Si ₃ N ₄	40–60	3.2
TiC	40–50	2.25
Al ₂ O ₃	40–340	4.0
B ₄ C	40–300	2.5
ZrO ₂	75–180	5.65–6.15
BN ₂	40–50	2.25
Graphite	40–250	1.6–2.2

Table 2.3 Properties of whiskers used in MMCs (Stacey 1988)

Whiskers	Length, l (μm)	Diameter, d (μm)	Density (g/cm^3)	Ultimate tensile strength, UTS (GPa)	Modulus of elasticity (GPa)
SiC (Tokai)	50–200	0.1–1	3.2	3–14	400–700
SiC (Arco)	50	0.2–1	3.2	13	700
Al ₂ O ₃	100	2	3.97	14	2,275
Si ₃ N ₄	5–200	0.1–1.6	3.18	13.8	379
Al ₂ O ₃ -B ₂ O ₄	10–30	0.5–1	2.93	8	400

of the commonly used discontinuous reinforcements (Giro et al. 1987; Stacey 1988). The reinforcement of particles have gained major interest as they enable obtaining a strong enhancement of mechanical properties while maintaining an isotropic behavior, with relatively simple production routes (Maruyama 1998; Miracle 2005) and a possibility to use secondary processes (Ellis 1996; Manna and Bhattacharayya 2003). Whiskers are elongated single crystals that have a high degree of structural and chemical perfection and provide high strength and

Table 2.4 Properties of short discontinuous fibers used in MMCs (Stacey 1988)

Fibers	Length, l (μm)	Diameter, d (μm)	Density (g/cm^3)	UTS (GPa)	Modulus of elasticity (GPa)
Carbon T300	2.5	7.8	1.75	3.45	230
SiC (Nicalon)	1–6	10–16	2.55	3	195
Al_2O_3 FP	3–6	15–25	3.96	1.7	380
Al_2O_3 Saffil	–3	1–5	3.30	2	300
Saffil HA	0.1–3	1–5	3.40	1.5	300
Fiberfrax	1–3	1–7	2.73	1.5	105
Alumino silicate	2–5	1–7	3.00	0.8	150

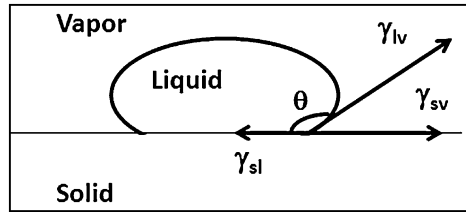
modulus of elasticity. Short/discontinuous fibers have much lower l/d ratio than continuous fibers. Both discontinuous fibers/particles have the following unique features when used as reinforcements.

- Isotropic properties
- Easy fabrication by conventional methods
- Sustainability of high operating temperatures
- Increased modulus of elasticity and strength
- Increased thermal stability
- Increased wear resistance
- Less expensive (cost-effective)

Recently nano-sized reinforcements (SiC, Al_2O_3 , B_4C , etc., of size usually <50 nm) have been used. Carbon nanotube (CNT) is also a promising reinforcement. The major advantage of using nano-reinforcements is that the enhancement in properties (including ductility) can be attained at lower volume fractions (<2 %), whereas for micron-scale particle reinforced MMCs higher volume fractions ($\gg 10$ %) are required. However, in order to produce sound nanocomposites with enhanced mechanical properties, good dispersion of the nano-reinforcement phase within the matrix is necessary, which is in turn strongly governed by the selection of a suitable production process.

Interface. Metcalfe (1974) defined the interface in a composite as “a surface formed by the common boundary of reinforcement and matrix in contact, which constitutes the bond in between for the transfer of loads.” The interface has physical and mechanical properties which are unique and not that of either the fiber/particle or the matrix. The interface occupies a large area in the composite. Being in between the matrix and the reinforcement, the interface is thermodynamically unstable, and exerts an influence on the overall performance of the composite. It is to be further noted that the interface causes a large discontinuity in material parameters such as the modulus of elasticity (E), coefficient of thermal expansion ($\text{CTE}-\alpha$), and the chemical potential of a composite. Such a difference, e.g., in the CTE between the reinforcement and the matrix, would cause a residual stress field and would affect

Fig. 2.1 Schematic diagram showing the contact angle between a liquid and solid surface. When
 (a) $\theta = 0^\circ$ —perfect wettability,
 (b) $\theta = 180^\circ$ —no wetting, and
 (c) $0^\circ < \theta < 180^\circ$ —partial wetting



the properties in many complex ways. Similarly, a chemical potential discontinuity would lead to interdiffusion zone. This would provide preferential sites for any segregation and precipitation.

2.2.1 Importance of Interfacial Bonding

The basic requirement of a composite is the intimate contact and efficient bonding between the matrix phase and the reinforcement phase. Such a bond would provide required efficiency in load transfer, usually from the matrix to the reinforcement. The factors influencing the qualities of an interfacial bond are briefly discussed below.

Wettability. Wettability is the ability of a liquid to spread on a solid surface. It is dependent on the contact angle attained, which describes the extent of intimate contact between a liquid and solid. In composites, the wettability is measured by the amount of work required by the molten metal to engulf the solid reinforcement. A contact angle between the liquid (molten metal) and the solid surface (reinforcement) close to 0° indicates perfect wetting, while the angle 180° indicates nonwetting (Fig. 2.1). The wettability, therefore, indicates the possibility of realizing an intimate contact between the liquid and the solid constituents in the composite (Mortenson et al. 1988). As most of the metal/reinforcement systems in MMCs show poor wettability, various measures have been attempted to improve wettability. Some such measures are pretreatment of reinforcements, alloying modifications, and coating of reinforcements (Krishnan et al. 1981; Kimura et al. 1984; Rohatgi et al. 1986; Delanney et al. 1987).

Mechanical bonding. Mechanical bonding occurs due to the mechanical-keying effect between the surfaces. Increasing the surface roughness of the reinforcement usually produces such mechanical-keying effect. Rough surfaces could be achieved by the process of etching. One such example was observed in W/Al composite (Metcalf 1974) where etching of tungsten wires was carried out to produce a rough interface in the composite. This caused the desired mechanical bonding and increased the stress levels. Artificially produced interface roughness by etch pitting or by microhardness indentations are some of the other methods employed to improve mechanical bonding (Chawla and Metzger 1978).

Chemical reactions. The chemical gradient across the reinforcement-matrix interface (produced under favorable conditions) would cause diffusion to occur or may cause chemical reactions between the components. The interface layer thus formed would then have characteristics that are much different from the individual constitutive components (Metcalf 1974). Occasionally, these would prove beneficial and facilitate an improvement in the nature of the bond between the reinforcement and the matrix. This however depends on the critical thickness of the interface layer above which the effect is adverse. In most cases, the interfacial chemical reactions result in brittle oxides/carbides/intermetallics which act as local stress concentrators resulting in the brittle behavior of the composite.

Thermal stresses. Apart from wettability, mechanical bonding, and chemical effects, thermal stress is yet another important factor that affects the interfacial bonding. The linear coefficient of thermal expansion (CTE) of the metal matrix is usually higher than that of the ceramic reinforcement. Such thermal incompatibility (mismatch) between the matrix and the reinforcement leads to the formation of a large thermal residual stress field along the interface, which affects the characteristics of the composite in a complex manner. If the stresses so produced were of the order of the yield stress of the matrix metal, then it would cause local plastic deformation. This deformation would then introduce dislocations and vacancies at the interface; subsequently responsible for activating chemical reactions at those sites. The thermal mismatch is also believed to accelerate the precipitation kinetics of the matrix. Evidences of the existence of a hard zone of high dislocation density around the reinforcement and a soft zone of low dislocation density away from the reinforcement have been observed due to the thermal mismatch across the interface. This influences the property of the matrix, leading to a strengthening effect in nonprecipitation hardenable alloys and accelerating the aging kinetics in precipitation hardenable alloy systems (Metcalf 1974). Often such thermal mismatch would result in localized plastic deformation (inhomogeneous deformation in the composite).

2.2.2 Role of the Metallic Matrix

As mentioned earlier, the matrix plays an important role in the behavior of the composite. The matrix not only holds the reinforcements (fibers/particles) and aids in the transfer of load to the reinforcements, but also affects the overall performance of a composite. The chemical and thermal reactions of the matrix with the reinforcement result in a change in the matrix microstructure that would then alter the properties of the composite. The two factors that influence the matrix behavior are the following:

1. The difference in the CTE at the reinforcement/matrix interface (due to the thermal mismatch between them) leads to the formation of residual stress zones.
2. The chemical incompatibility at the reinforcement/matrix interface forms a new chemical zone. This new zone will have a CTE which is different from that of the matrix and the reinforcement making the overall behavior and response of the

system more complicated. Possible events that are predictable from such reactions that are induced into the matrix are (Metcalf 1974):

- (a) Plastic deformation mechanisms such as slip, twinning, grain boundary sliding, and grain boundary migration, in the case of ductile matrix.
- (b) Cracking and failure in the case of brittle matrix.
- (c) Failure at the reinforcement/matrix interface in both kinds of matrices.

2.3 Processing of LMMCs

LMMCs manufacturing processes are classified into ex situ routes, when the reinforcing phase is produced at an earlier stage and then added to the matrix, or in situ routes, when the reinforcement is generated during the composite production, typically through controlled reactions (Fridlyander 1994; Ye and Liu 2004; Tjong 2007). Ex situ processing techniques are commonly employed to make LMMCs and can be further classified into liquid, solid, and semisolid state processes. Some of these production routes are also suitable for nanocomposites production. The choice of the processing route depends on several factors such as the reinforcement type, its distribution, matrix-particle bonding, control of matrix microstructure, process simplicity, and cost-effectiveness. The ex situ processing routes are described below.

2.3.1 Liquid-State Processes

Liquid-state processing routes are attractive as they are relatively simple, cost-effective, and are potentially scalable to industrial level. These routes include stir casting, ultrasonic-assisted casting, centrifugal casting, infiltration techniques, and disintegrated melt deposition (DMD) method.

2.3.1.1 Stir Casting

Stir casting is also known as the vortex method and is widely used to produce LMMCs. It involves incorporation of reinforcements (mainly in the form of particles) into the molten metal, followed by casting. Homogenous distribution of reinforcement is achieved by:

1. A rotor rotating in the liquid metal that creates a vortex or
2. By injection of a gas carrying the reinforcement into liquid metal (Fig. 2.2) (Ezatpour et al. 2014)

The finely distributed slurry so produced is shaped by conventional casting techniques, viz. sand casting, permanent mould casting, pressure die casting or squeeze casting (Evans et al. 2003; Noguchi et al. 2008).

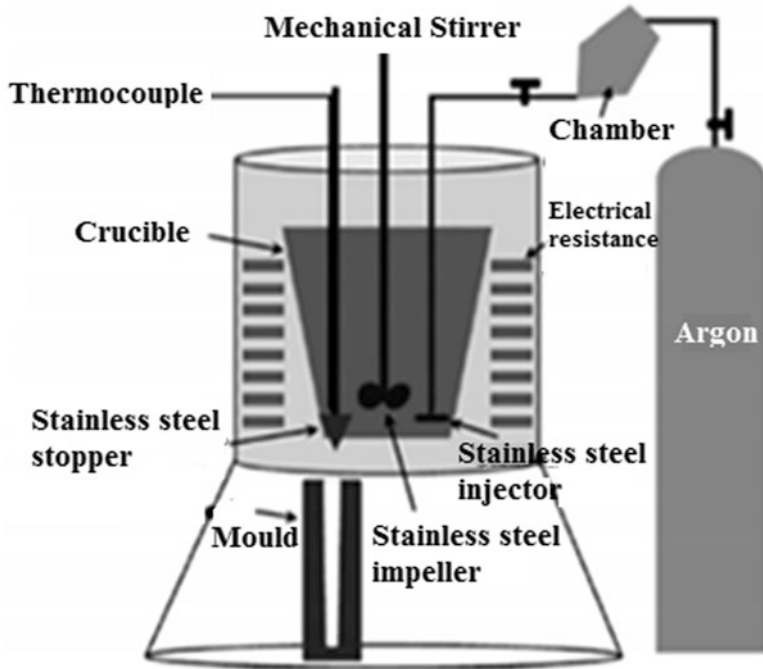


Fig. 2.2 Stir casting (vortex) method (*adapted from Ezatpour et al. 2014*) (© 2014, Elsevier. Used with permission). This method is cost-effective, simple, and effective in producing nanocomposites

Issues associated with stir casting process are: (1) gas entrapment and (2) slag in the melt. These lead to high porosity and microdefects. (3) Undesired chemical reactions at the matrix/reinforcement interface and (4) low wettability of reinforcements with the molten matrix that increases the tendency of the particles to agglomerate (especially in nano-reinforcements that could result in the formation of nanoparticle clusters and nonuniform distribution of reinforcement). These issues if unchecked would cause severe deterioration of material properties. To successfully implement this process at both laboratory and industrial scales, careful standardization of process parameters such as temperature of molten metal, melt stirring time, stirring velocity, melt holding temperature, choice of matrix-reinforcements, etc., should be rightly selected (Koli et al. 2013).

2.3.1.2 Centrifugal Casting

Centrifugal casting is a relatively inexpensive process in which optimal reinforcement placements are achieved by inducing a centrifugal force immediately during casting (Fig. 2.3, <http://www.adityainc.com/casting/centrifugal-casting.html> 2014).

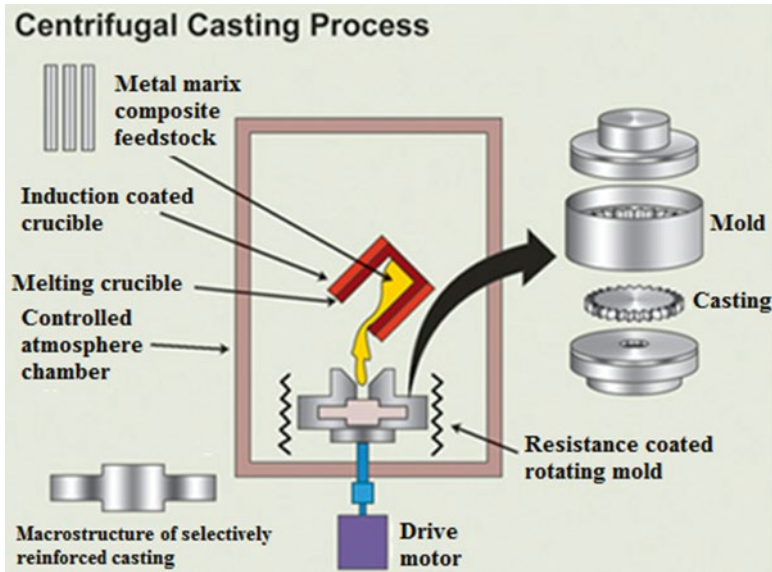


Fig. 2.3 Schematic of centrifugal casting process (<http://www.adityainc.com/casting/centrifugal-casting.html> 2014). Last accessed 23 Oct 2014

This ensures an intentional variation in volume fraction (functionally gradient) within the matrix material. A typical example for use of centrifugal casting is in brake rotors, wherein the rotor face is expected to be of high wear resistance when compared to the hub. When processed by regular casting methods, difficulties in machining are encountered due to the high hardness of the composite; these are eliminated by centrifugal casting process (Chawla and Chawla 2006).

2.3.1.3 Squeeze Casting/Infiltration Process

This process involves the infiltration of a molten alloy into a ceramic fiber/particle preform followed by solidification (Ghomashchi and Vikhrov 2000). The introduction of molten metal into a preform could be achieved either through pressureless infiltration or by infiltration under pressure. In pressureless infiltration, ceramic fiber bundles are first placed in the die. The molten metal is then poured on to it and allowed to solidify. The solidified composites are then hot pressed to achieve 100 % density. The initial infiltration occurs without any application of external pressure and the wettability of fibers ensures efficient infiltration. The pressure infiltration process can be employed in two different ways, namely via gas infiltration and pressure infiltration. In gas infiltration, vacuum or inert gas atmosphere is utilized to bring forth infiltration. Advantages of this method include increase in the wettability due to the increased surface activity of reinforcement in vacuum environment,

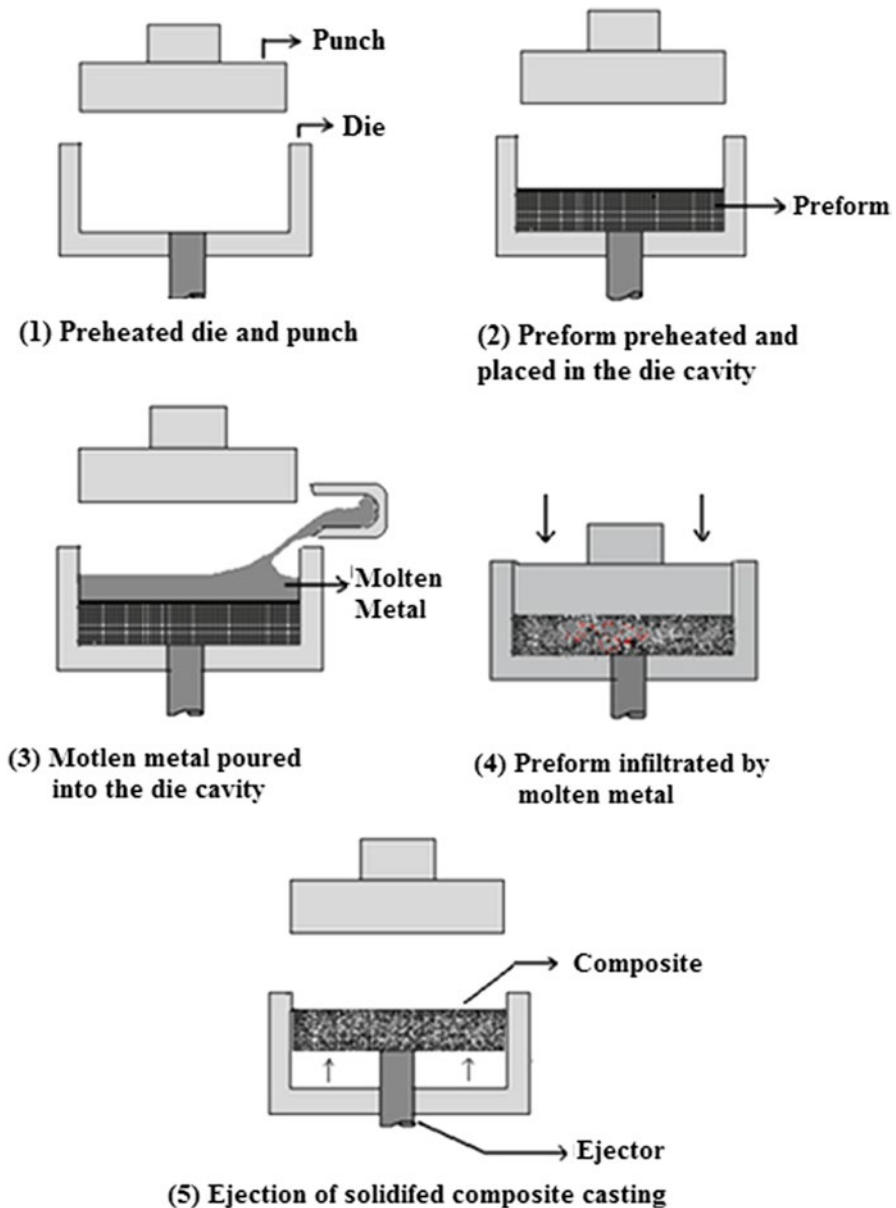


Fig. 2.4 Schematic of squeeze casting/infiltration process

elimination of gas entrapment or porosity and achieving near-net shaped components. Its main disadvantages are segregation of phases and reaction between matrix/fiber due to the slow nature of the process.

The squeeze infiltration process involves the infiltration of molten metal into a ceramic preform using hydraulic pressure (Fig. 2.4). By this method, the drawbacks

of phase segregation and matrix/interface reaction encountered in gas infiltration can be eliminated due to the application of hydraulic pressure (as it increases the solidification rate). To note, preforms are usually prepared using ceramic reinforcements having aspect ratios (e.g., alumina short fibers). For nanoscale reinforcements, CNTs are used as preforms for they have dimensional anisotropy (i.e., aspect ratio) (Uozumi et al. 2008). However, preparation of CNT preforms is a major challenge. In both cases, an improperly made preform can cause local inhomogeneous distribution of reinforcement fibers causing large variation in the volume fraction within a solidified composite. Also, in case that the preform is not well prepared (such as insufficient binder), it has a tendency to break during the application of squeeze pressure.

Squeeze Casting/Infiltration Process Parameters

The quality of composite castings produced in this process largely depends upon the control of the processing parameters discussed below.

1. *Metal casting temperature*: The temperature at which the metal is poured into the die cavity plays an important role on the casting quality and die life. The casting temperature depends on the liquidus temperature, the freezing range of the alloy, and the die configuration. Low casting temperatures result in inadequate fluid life and incomplete die fill. On the other hand, high casting temperatures would force the metal to penetrate between the die and punch leading to metal flash or jamming of the tooling.
2. *Tooling temperature*: High tooling temperatures would cause surface defects in the castings. In some cases, welding may occur between the casting and the die wall. Low temperature leads to premature solidification, thermal fatigue, and cold laps. Temperatures of $\sim 300^\circ\text{C}$ or less are maintained for nonferrous alloys.
3. *Melt quality and quantity*: In this process, the metal is directly poured into the cavity that has no gating or feeding system. Hence adequate precautions should be taken to ensure that the material is free from any dross or suspended impurities. Due to the absence of a gating system, the process requires precise quantity of metal to be poured into the die cavity, which will otherwise change the casting dimensions.
4. *Die coating/lubricant*: Die coating serves as a releasing agent and is selected based upon the die material and the alloy composition. A commonly used die coat is water-based colloidal graphite that is sprayed onto the die surface and the punch. At high squeeze pressures, the coating may get stripped from the die surface causing surface contamination. Hence, precaution should be taken in applying the coating to the right thickness to ensure its desired performance.
5. *Temperature for pressure application*: The squeeze casting/infiltration process is fully effective when the metal is completely in a liquid state (Das and Chatterjee 1981). Hence, the control of time delay between pouring and squeezing is very important and should be minimized. Else, it may lead to reduction in the melt temperature leading to premature solidification or incomplete infiltration of the preform.

6. *Duration of pressure and pressure level*: The applied pressure level depends on the fluidity and the freezing range of the alloy (Das and Chatterjee 1981). It also depends on the component geometry and the alloy characteristics. Pressure in the range of about 30–110 MPa is usually required to eliminate gas or shrinkage porosity. The duration of pressure application depends on the alloy type and the heat transfer conditions. Prolonged holding under pressure would cause die wall cracking and difficulty in the withdrawal of the punch. A high applied pressure may also result in breakage of the preform. Usually, a maximum pressure holding time of approximately 1 s/mm section thickness of casting is employed.
7. *Press speed*: At high press speeds, the following may occur: metal flash at joints, dilation of die parts and premature solidification at the impact zones due to instantaneous peak pressures. Normally a two-speed action of rapid approach to the metal surface followed by a slower impact speed is adopted.
8. *Preform properties*: Major factors to be considered are the full infiltration of the preform (without damage or distortion) and the freezing of metal in the preform with good interfacial contact between the matrix and the fiber. Insufficient infiltration produces shrinkage pores that deteriorate the properties of the composite. Further, the degradation of fibers by the melt depends on the exposure time, squeeze infiltration temperature, wettability, and the bonding between the fiber/matrix at the interface. In addition, nonuniform distribution of fibers (clustering) and large increase in applied pressure result in fiber degradation.

2.3.1.4 DMD Technique

The DMD technique is a liquid-state processing method, which has the combined advantages of both gravity die casting and spray forming processes (Gupta and Sharon 2011). Unlike in the spray process, DMD employs higher superheat temperatures and lower impinging gas jet velocity. It is usually employed for particle reinforcements, and is quite successful for reinforcing nanoparticles. The process involves stirring of reinforcement particles with a predetermined stirring velocity and time using an impeller when the metal/alloy is in the molten state. The resulting composite slurry is then made to exit from the bottom of a crucible, followed by disintegration of the melt by jets of inert gas at a superheat temperature of 750–850 °C (depends on the alloy) and is finally deposited onto a metallic substrate (Fig. 2.5). The disintegration process of the composite melt ensures higher solidification rate and fine-grained structure.

Generally during Mg materials production via conventional methods such as gravity die casting, critical issues encountered are:

1. Presence of oxides in the final product (molten Mg is highly oxidizable in nature)
2. Retention of reinforcement particles in crucibles (i.e., most of the reinforcement particles are denser than Mg, and hence tend to settle at the bottom of crucibles)

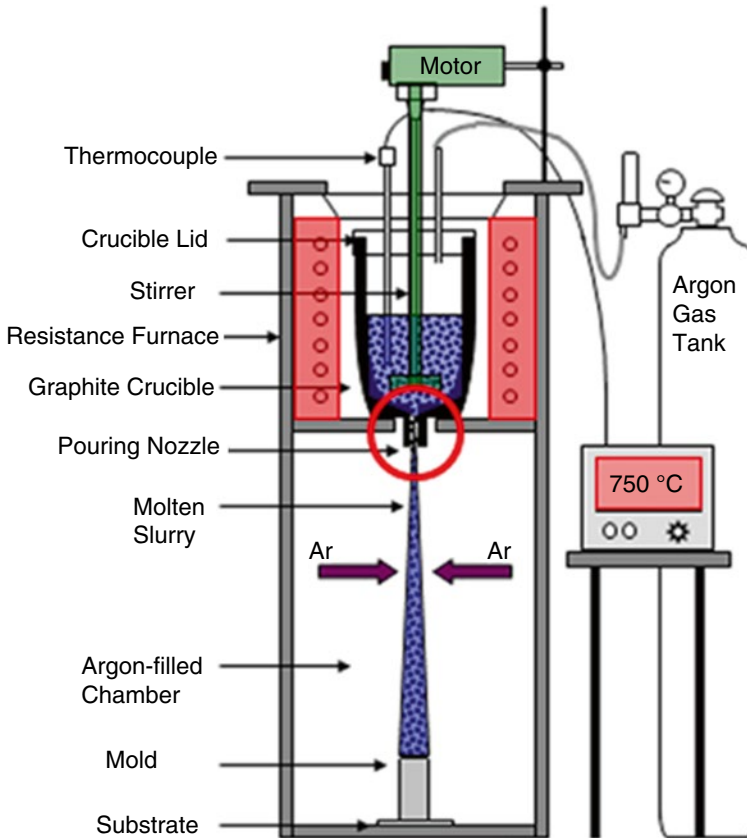


Fig. 2.5 Disintegrated melt deposition technique. This method has the advantage of both conventional die casting and spray forming processes. It is very suitable to produce Al- and Mg-based nanocomposites

These together give rise to impurities, insufficient reinforcement volume fraction, and nonuniform reinforcement dispersion. Given that DMD is a bottom-pouring technique, it ensures:

1. Effective elimination of oxide entry into deposited products
2. Complete utilization of the reinforcement
3. Higher solidification rates due to disintegration of molten metal by inert gas

Salient features of the process are:

- Combined advantages of casting and spray forming processes.
- Eliminates the requirement for separate melting and pouring units.
- Removes oxides and slag/dross and least metal wastage.
- Flexibility of addition/incorporation of alloying/reinforcing particle elements.
- Eliminates the retention/settling of the reinforcements in the crucible.
- High process yield and gives rise to fine-grained materials with minimal porosity.

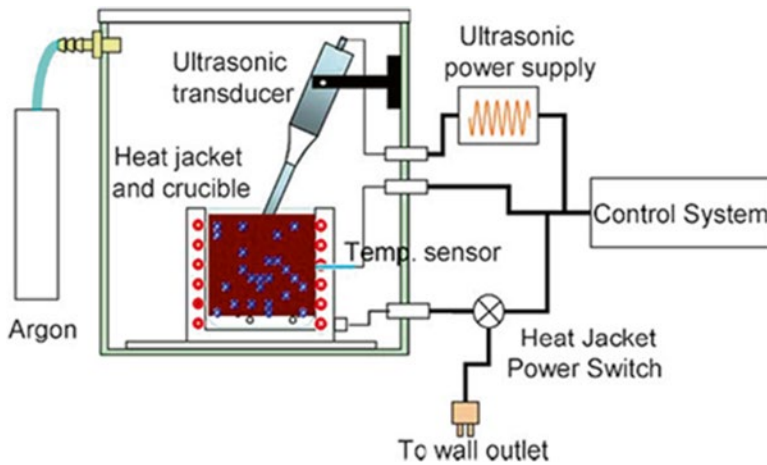


Fig. 2.6 Schematic of Ultrasonic-assisted casting (*adapted from* Yang et al. 2004) (© 2004, Elsevier. Used with permission). The method is very effective to homogenously disperse nano-sized reinforcements in light metal matrices

DMD is a primary process, after which a secondary process such as extrusion is usually employed. Following this process, light metal composites/nanocomposites have been successfully produced at laboratory scale. To make components/products directly using DMD, the disintegrating gas velocity and the distance between the melt exit stream and a substrate need to be standardized according to the required dimensions of the final product/component. This being arduous, the process has remained suitable to produce composite ingots, which can then be used as precursors for making wrought products.

2.3.1.5 Ultrasonic-Assisted Casting

The ultrasonic-assisted casting method is effective in mitigating particle cluster formation in composites that occurs (nanocomposites in particular) due to the low wettability and high tendency of agglomeration of nanoparticles (Donthamsetty et al. 2009; Mula et al. 2009). Agglomeration is usually encountered in conventional stirring methods such as mechanical stirring/vortex methods. In contrast, the ultrasonic-assisted method employs subjecting the melts with ultrasonic waves (frequency range: 18–20 kHz) during or after adding a reinforcing phase. This is followed by casting. A schematic of the setup is shown in Fig. 2.6 (Yang et al. 2004).

High-intensity ultrasonic waves can generate transient cavitation and acoustic streaming in liquids (Abramov 1994). Acoustic streaming causes pressure gradient within the bulk of molten metal that produces stirring effect. In cavitation, cyclic high-intensity ultrasonic waves induce the formation, growth (during the negative pressure cycle), pulsating, and collapsing (during the positive pressure cycle) of tiny bubbles in the liquid phase. At every cavitation cycle, bubbles implisively collapse

in less than 10^{-6} s, producing micro “hot spots” that can reach temperatures of $\sim 5,000$ °C, pressures of $\sim 1,000$ atm, and heating/cooling rates $> 1,010$ K/S during microseconds transient (Suslick et al. 1999). During cavitation of the composite melt, the air entrapped in voids of particle clusters serves as nuclei for cavitation, which is strong enough to break the clusters thereby providing uniform dispersion. The high pressure and temperature developed also removes gases/impurities and enhances the wettability of the reinforcement with matrix. This method is extremely successful in producing composites with uniform dispersion of nano-reinforcements, at laboratory scale. For any large-scale production, it requires to up-scale the probe size with higher source power to ensure its effect over large volume of melts.

2.3.1.6 High Pressure Die Casting

Among the traditional liquid processes, aside from stir casting technique, high pressure die casting (HPDC) has also been used for LMMC production. In general, the process enables obtaining more precise components as compared to gravity and low pressure die casting methods. The molten metal is forced into the die cavity under pressure, and both filling speeds and solidification rates are particularly high. For this reason, HPDC method is characterized by fast cycle times, which may range from seconds to several minutes, depending on the size and wall thickness of the casting. On the other hand, the process inevitably induces gas entrapment due to the highly turbulent flow of metal in the cavity (Wang et al. 2011; Long et al. 2012). Very few works have been reported on the application of HPDC for the production of MMCs, especially in the case of nanocomposites. HPDC was applied by Li et al. (2010) to manufacture CNT-reinforced Al-based composites. The composites exhibited an increase of both tensile stress and elongation to failure when compared to the unreinforced alloy.

2.3.2 Solid State Processes

Solid state processes involve production of materials in solid state form (such as powders in powder metallurgy (PM)) (Suryanarayana and Al-Aqeeli 2013). The first step in powder metallurgy method is the blending/mixing of metal matrix and reinforcement powder, which is conducted using a ball-milling machine (without milling media, e.g., steel balls). In some cases, reactive mixing is employed, in which reinforcement particles and/or the alloying/catalyst element are milled together (with a milling media at selected rpm and time duration). This step is undertaken so as to improve the wettability. The powders so blended are then compacted usually by cold pressing (called “green compacts”), and in some cases by using hot/vacuum hot pressing. The green compacts are then further sintered using either of the methods of direct sintering using resistance furnace, microwave-assisted sintering, spark plasma sintering, hot extrusion, severe plastic deformation, etc.

PM methods can be used for producing near-net shaped composite components and large-batches of small components. As the various PM processes are exhaustive, only a brief mention on the process, microstructure, and mechanical properties are presented in this chapter. For more detailed information, the readers can refer to Suryanarayana and Al-Aqeeli (2013), which deals exclusively on solid state processes and properties of composites. Major advantages of PM techniques are:

1. Minimal wettability-related problems
2. Incorporation of higher volume fraction of reinforcements
3. Possibility of using reinforcement-metal combinations not viable by liquid-state routes

Some of the drawbacks include cost-ineffectiveness, oxidization of powders which demands inert/protective gas conditions, and high porosity content (inevitable in powder metallurgy techniques) that leads to degradation in properties, especially the drastic reduction in ductility. As a part of PM process, sintering of green compacts is usually performed using conventional resistance furnaces. Other techniques such as microwave-assisted rapid sintering and spark plasma sintering (SPS) have also been recently developed and are being used to produce composites and have been briefly mentioned.

2.3.2.1 Mechanical Alloying

In the traditional PM process, the aim of blending is simply to mix the powders without inducing material transfer between the mixed components. It is possible, however, to perform a high energy mixing through milling media, so as to eliminate the voids between the matrix and the reinforcement powders through a solid state bonding (Ye et al. 2005). For example, in mechanical alloying (MA), matrix and reinforcement are alloyed together by inducing cold welding, fracturing, and re-welding of the powder particles (Suryanarayana 2001, 2011; Suryanarayana and Al-Aqeeli 2013). The strengthening of metallic alloys is achieved through grain size refinement and dispersion of particles. During the process, a small quantity of the base powder is loaded into a sealed container, together with the grinding media, then blended through agitation at high speed for a predetermined amount of time (Fig. 2.7a). As the kinetic energy of the grinding balls depends on their mass and velocity, dense materials such as stainless steel or tungsten carbide are preferred to ceramic. Main process parameters, influencing the quality of the composite, comprise ball-to-powder ratio (BPR), time and rotational speed of milling. After being milled, powders are compacted, degassed, and consolidated.

A process control agent (PCA, usually referred to as lubricant or surfactant) is usually added while blending the powders, aimed to minimize the effect of cold welding and consequent formation of large powder clusters. Methanol, stearic acid, and paraffin compounds are used for this purpose (Witkin and Lavernia 2006). During continuous severe plastic deformation, refinement of the internal structure of the powders to the fine scales may occur, resulting in the production of

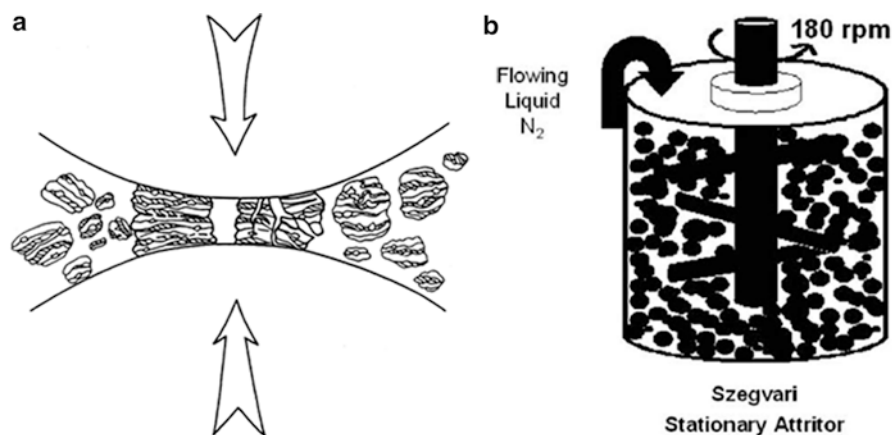


Fig. 2.7 (a) Mechanical alloying processing technique: milling action on the powders (*adapted from Suryanarayana 2001*) (© 2001, Elsevier. Used with permission). (b) Schematic of cryomilling process (*adapted from Witkin and Lavernia 2006*) (© 2006, Elsevier. Used with permission)

nanostructured powders (Fecht 1995; Suryanarayana 2011). In the entire process, contamination of the powders must be carefully controlled. Possible sources of contamination are the milling tools, milling atmosphere, as well as the PCA. During consolidation, impurities may influence microstructural evolution and grain growth, leading to a possible decrease of mechanical properties of the resulting composite. In some cases, the milled powders obtained from mechanical alloying are also employed as reinforcing particles for casting processes.

2.3.2.2 Reaction Milling

Mechanical alloying can also be accompanied by a solid state reaction, aimed to produce fine dispersion of oxides, nitrides, and carbides in the light alloy matrix. In this case, the process is usually defined as reaction milling (RM). In order to allow the reaction to occur, the PCA can be absent or a suitable milling atmosphere can be used to introduce reagents, i.e., oxygen, argon, nitrogen, or simply air (Suryanarayana 2001). Sometimes the PCA could be itself part of the reaction process.

2.3.2.3 Cryomilling

In cryomilling, the milling phase is carried out at cryogenic temperatures (Fig. 2.7b) or, in some cases, within a cryogenic medium, as liquid nitrogen (Witkin and Lavernia 2006). A PCA (e.g., stearic acid) can be used to avoid severe sticking. During traditional milling process, the temperature increases due to the attrition. As a result, severe recovery and recrystallization of fine microstructures occur.

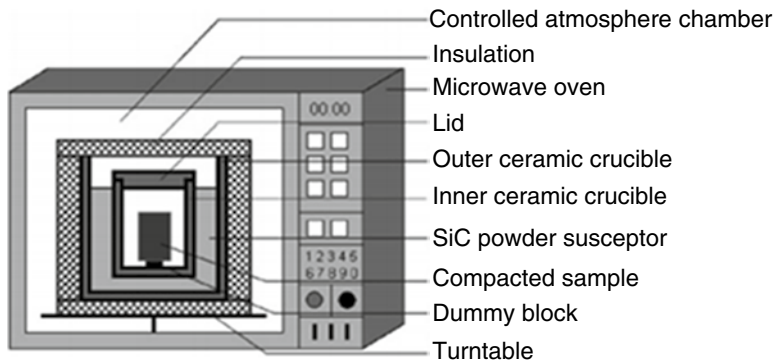


Fig. 2.8 Bi-directional hybrid microwave-assisted rapid sintering (*adapted from Tun and Gupta 2009*) (© 2009, Elsevier. Used with permission). This technique is advanced than conventional sintering in terms of distribution of heat during sintering and energy efficiency

On the contrary, when cryomilling is applied, recovery and recrystallization are suppressed by the extremely low milling temperature, enhancing the beneficial effects of mechanical milling and leading to finer grain structures and more rapid grain refinement. As a result, grain structures of the order of nanocrystallites may be obtained. Moreover, detrimental chemical reactions between matrix and reinforcement are also suppressed at such low temperatures.

2.3.2.4 Microwave Sintering

Microwave heating is a volumetric heating process that involves the conversion of electromagnetic energy into thermal energy (Gupta and Eugene 2007). In conventional sintering processes, during sintering, the thermal energy is transferred from the outer surface of materials to their inner surface. In contrast, in microwave sintering, heat is generated from within the materials. It is then radiated outwards due to the penetrative power of microwaves. Due to this phenomenon, during microwave sintering, higher temperatures exist at the core of materials whereas their surfaces experience lower temperatures (thermal gradient), which results in variation of microstructure and hence the properties. To avoid such an occurrence hybrid microwave heating referred to as the “bi-directional hybrid microwave-assisted rapid sintering” has been developed (Fig. 2.8) (Tun and Gupta 2009).

In this process, microwave susceptors such as SiC particles/rods are used to assist in the reduction of thermal gradient during sintering. The compacted metal/composite powder billets are placed in the inner crucible and SiC powder is placed in between the inner and outer crucibles. As SiC powder absorbs microwave readily, it heats up quickly. This provides radiant heat that can in turn externally heats the compacted billets. In addition, the compacted billets themselves absorb microwave and get heated from within/internally. Thereby, uniform heat is experienced along

the entire section of a specimen, thus reducing any core-to-periphery thermal variation (Gupta and Eugene 2007). Due to this reason, high sintering temperatures ($\sim 620\text{--}650\text{ }^{\circ}\text{C}$) can be generated within a short period of time (12–14 min), that are almost close to the melting points of Al and Mg, by the virtue of which enhanced wettability and reduced porosity can be achieved. The bi-directional hybrid microwave-assisted rapid sintering has been successfully used for nanocomposites production, especially for Mg materials. Advantages of this process include:

1. Rapid heating rates
2. Low sintering time due to which in most cases (even for Mg) the process does not require inert atmosphere
3. Lesser porosity when compared to conventional sintering
4. Fine microstructures and improved mechanical properties (Gupta and Eugene 2007)

2.3.2.5 Spark Plasma Sintering

As mentioned before, the main drawback of conventional sintering is the occurrence of high porosity in a product; likewise, when the green compacts are hot pressed, hot extruded, or hot isostatically pressed, it often results in matrix grain growth that weakens mechanical properties. In this regard, SPS, also known as field assisted sintering (FAST), is an effective nonconventional sintering method for obtaining fully dense materials with refined grain size (Saheb et al. 2012). In SPS, the densification is facilitated by the use of a current. A pulsed DC current is directly passed through a graphite die and composite powder compact. Joule's heating effect plays the role in densifying powder compacts achieving near theoretical density. In SPS, the heat generation is internal in contrast to the conventional hot pressing (where heat is provided by external heating elements). This facilitates high heating rates (up to $\sim 1,000\text{ K/min}$) and hence the sintering process is very fast (within a few minutes). The speed of the process ensures densification of powders while avoiding coarsening that occurs in standard densification routes (Saheb et al. 2012; Sairam et al. 2013). Figure 2.9 shows a SPS process setup (Saheb et al. 2012). A detailed review on SPS process can be found in ref. Saheb et al. (2012).

2.3.3 Semisolid State Processes

In semisolid processes, incorporation of particles in matrix metal is conducted when a matrix is in semisolid state (slurry), as it:

1. Facilitates uniform dispersion of reinforcements
2. Eliminates settling of denser reinforcement due to slurry state
3. Eliminates porosity (that usually occurs due to voids generated at the molten metal/particle interface)

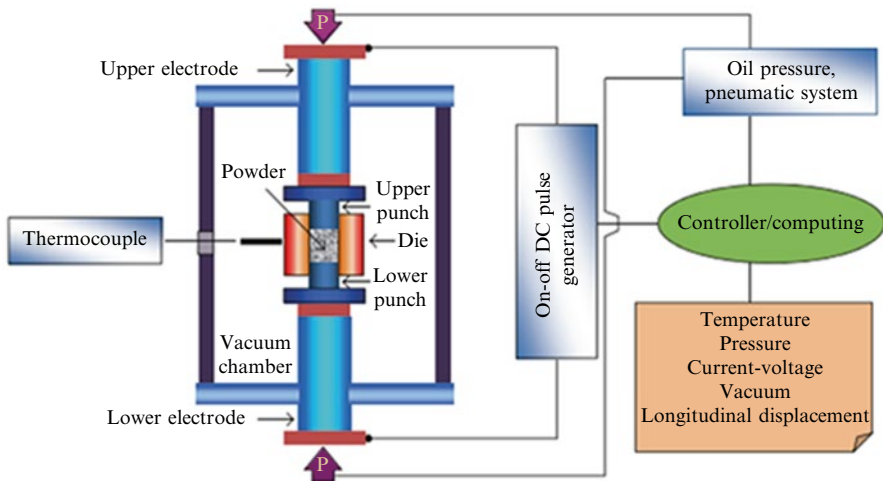


Fig. 2.9 Spark plasma sintering (SPS). This process is effective for producing fully dense light metal nanocomposites (*adapted from Saheb et al. 2012*) (©2012, Hindawi. Open access)

Semisolid processes are of two types, namely thixo-process/casting and rheo-processes (compcasting). In thixo-casting process, addition of particles is carried out in matrix molten state followed by agitation/vortex stirring of particles in slurry state, and then casting. In rheocasting, incorporation of nanoparticles is done in the semisolid state of a matrix. A combination of techniques such as semisolid processing (stirring) assisted by ultrasonic vibration has been utilized to achieve effective dispersion when using nano-reinforcements (Nie et al. 2011; Kandemir et al. 2012).

2.3.3.1 Thixo-processing

In thixo-processes a proper solid feedstock is reheated and partially melted. The base material is generated by allowing a liquid melt to partially solidify under controlled conditions (low superheat and rapid cooling, usually combined with significant convection in the liquid), so as to induce the formation of crystals in the slurry. The feedstock may be produced in a variety of ways such as with mechanical stirring during solidification as in rheocasting, continuous casting combined with magneto-hydrodynamic stirring for grain refining and ultrasonic treatment for grain refinement. Other methods to prepare fine-grained nondendritic material are by spray casting and low-superheat casting processes. Many of the processes employ intense chemical inoculation to maximize the efficiency of the above mentioned processes, particularly magneto-hydrodynamic stirring and low-superheat casting. Usually, the semisolid material is then injected into hardened steels, dies as final stage process. The advantages of semisolid processing include low shrinkage and porosity, nonturbulent filling and lower processing temperature (Abbasipour et al. 2010; Heinrich and Gonasagren 2012).

2.3.3.2 Rheo-processing

Unlike the thixo-process, in the rheo-processes a special feedstock is not required, and the semisolid slurry is generated starting from the liquid state by cooling the molten metal during the casting process itself. In common for all rheo-processes is that they are easier to implement in a foundry as they involve standard equipment for melting, transport, treatment, degassing, and handling. The key difference between the various approaches is in the slurry-making process, where great efforts are being made to create a robust on-demand slurry-making capability. Among rheo-processes techniques, it is worthwhile mentioning the New Rheo Casting process (NRC), which relies on a cooling slope to generate the initial slurry (Yasunori et al. 1996). In this process, the molten metal is poured at low superheat (about 10 K) onto the side of a holing cup and a large amount of very small crystals are formed. The slurry is then held for a pre-set time in the cup, allowing the crystals to grow and spheroidize without additional shearing or stirring. Just before pouring the temperature of the slurry is homogenized (Kaufmann and Uggowitzer 2001). As a variation to the precedent, the Hong-Nano Casting method (H-NCM) (Hong and Kim 2006), uses an electromagnetic field in the pouring and cooling stages. This modification helps in homogenizing the temperature and increases the overall heat transfer, resulting in fast cooling and copious nucleation—approximately 1,000 times higher than in the NRC process. Further, the Rheo Die Casting process (RDC), also known as Twin Screw Rheo Moulding (TSRM), involves the use of twin screws for mixing, providing a high amount of shearing. The molten metal is cooled at a controlled rate. The high level of shear is thought to break oxides into small, round particles which are well dispersed in the entire cast component. The slurry may be generated by letting the melt passing through a conversion reactor (a cooled copper or iron block with a twisting channel inside, causing the melt to cool and partially solidify under shear) in the so called Continuous Rheo-conversion Process (CRP). Other processes developed so far for semisolid metal processing are the Sub-Liquidus (SLC) and Semi Solid Rheo (SSR) casting processes, GISS process, Rapid Slurry Forming (RSF), Semisolid Metal (SSM), and ATS processes.

2.3.3.3 Compocasting

Compocasting route, is a rheocasting process that involves the injection of reinforcement particles into semisolid state alloys (Fig. 2.10). Compocasting is generally thought to be a processing route allowing to obtain quite uniform distribution of reinforcing particles, as well as to enhance particle wettability (Kamali Ardakani et al. 2014). It has been reported that the primary solid particles which are formed in the semisolid slurry are able to mechanically entrap the reinforcing phase and to prevent their gravity segregation, as well as to reduce their agglomeration tendency (Naher et al. 2005). Moreover, the lower porosity which is usually observed in experimental studies is attributed to the better wettability between the matrix and the reinforcement particles as well as the lower volume shrinkage of the matrix

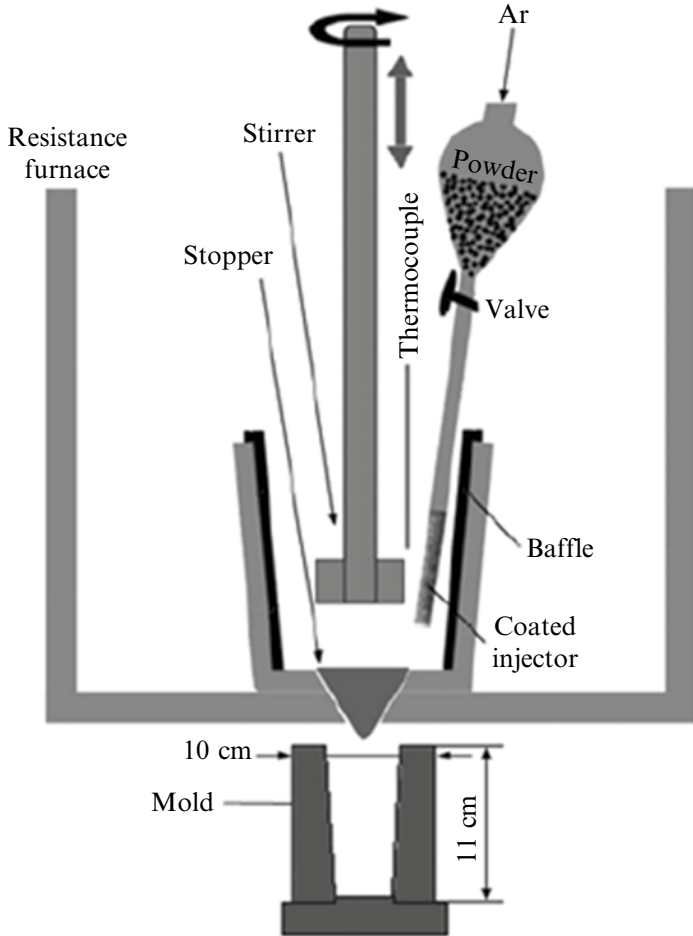


Fig. 2.10 Compocasting experimental setup (*adapted from Abbasipour et al. 2010*) (© 2010, Elsevier. Used with permission)

alloy. Despite these advantages, some agglomerates, inevitably induced by the high surface-to-volume ratio, as well as to Van der Waals interactions are still reported (Sajjadi et al. 2012).

2.3.4 Other Processes

Alternative processes to incorporate reinforcement particles into metal matrices to form bulk composites are also being developed. Friction stir process (FSP) is one such method, which is based on friction stir welding. Other processes are accumulative roll bonding (ARB) and equal channel angular pressing methods. These are severe plastic

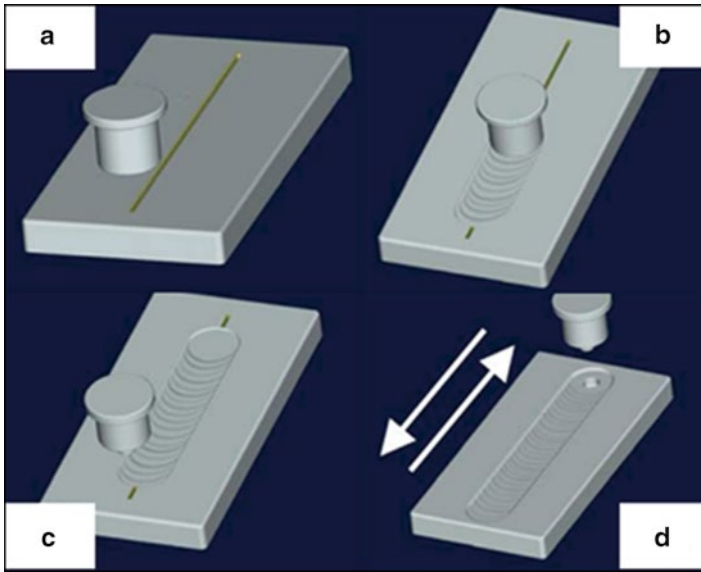


Fig. 2.11 Friction stir process (FSP): (a) cutting groove and inserting nanoparticles, (b) using a flat tool for surface repair, (c) applying a tool with a fixed pin that causes FS, and (d) conducting multiple FSP passes (*adapted from Lee et al. 2006*) (© 2006, Elsevier. Used with permission)

deformation (SPD) process used to produce fine-grained materials. Research on full utilization of these methods to produce LMMCs is in the developmental stage.

2.3.4.1 Friction Stir Processing

FSP is based on friction stir welding. It was initially used to produce surface-reinforced composites (Sun et al. 2012). During FSP, a rotating tool with a shoulder and a pin is plunged into the surface of a work piece (desired base matrix) with grooves filled with particles of required volume fraction (Fig. 2.11) (Lee et al. 2006). When the tool rotates, it covers the region of interest. In recent years, efforts are being made to use this process as an alternative route to incorporate nanoparticles into metal matrices to form bulk nanocomposites (Lee et al. 2006; Sun et al. 2012). However, obtaining uniform dispersion of nano-sized reinforcements still remains a challenge.

2.3.4.2 Equi-Channel Angular Pressing

Equi-Channel Angular Pressing (ECAP) is a SPD which involves processing/extrusion of a metal billet through an angled (typically 90°) channel (Segal 1999; Balog et al. 2013; Sklenicka et al. 2013) as shown in Fig. 2.12. To achieve optimal results,

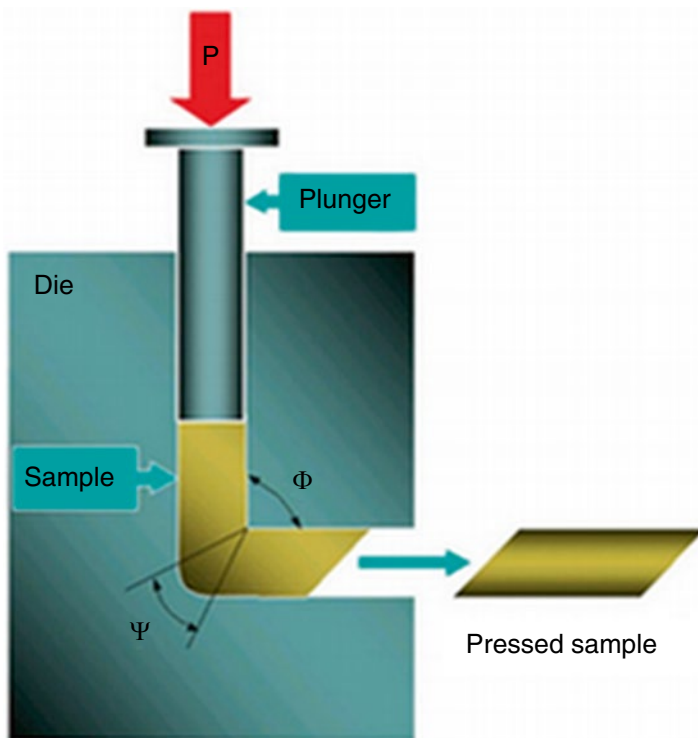


Fig. 2.12 Equi-channel angular pressing (ECAP). The die has an internal angle of 90° and an outer arc of curvature of $\sim 20^\circ$ (adapted from Sklenicka et al. 2013) (©2013, InTech. Open access)

this process is repeated several times, changing the orientation of a billet with each pass. This produces uniform shear throughout the bulk of material. The process is widely used for fine-grained/ultrafine-grained materials, and has also been adopted to produce nanocomposites as it can provide fine grains, uniform distribution of reinforcements, and elimination of porosity (Segal 1999).

2.3.4.3 Accumulative Roll Bonding

ARB is a solid state method in which composites can be produced in the form of sheets. This process is also an SPD process. In this process two sheets of the same material are stacked, heated (to below their crystallization temperature), and rolled to bind the sheets together (with up to 50 % thickness reduction) (Fig. 2.13) (Saito et al. 1999). The bonded sheet is then cut into half, the two halves are stacked together, and the entire process is repeated all over again several times. Compared to other SPD processes, ARB does not require specialized equipment or tooling, but only a conventional rolling mill. During the ARB process care should be taken to

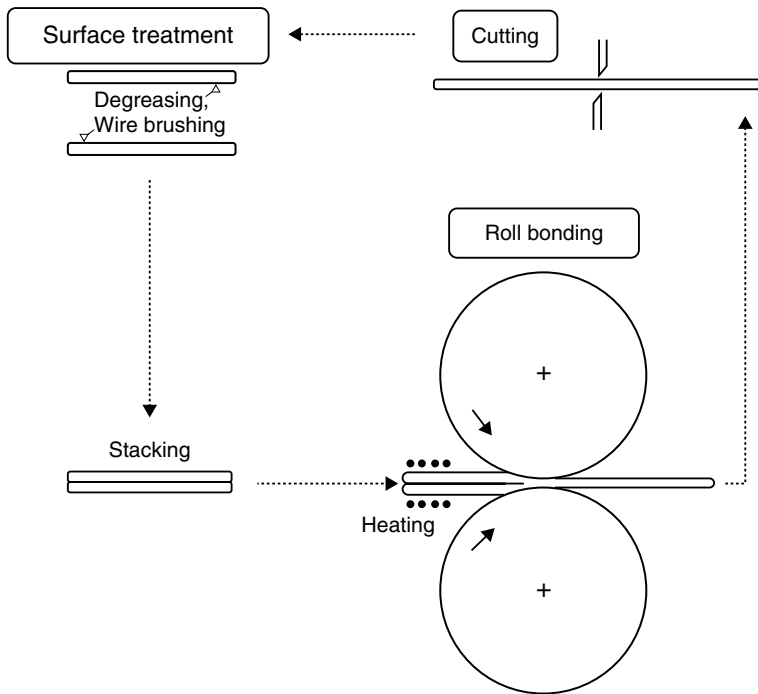


Fig. 2.13 Accumulative roll bonding (ARB) process, based on intense plastic straining (*adapted from Saito et al. 1999*) (© 1999, Elsevier. Used with permission). This process can produce nanocomposite in the form of sheets

thoroughly clean the surfaces before rolling them together so as to achieve good bonding (Saito et al. 1999).

2.4 Strengthening Mechanisms in LMMCs

For engineering materials design and selection, yield strength and ductility of a material are the most important parameters. These properties in LMMCs are enhanced by the strengthening mechanisms (Arsenault 1983; Nardone and Prewé 1986; Dieter 1988; Miller and Humphreys 1991; Brown and Stobbs 2006; Zhang and Chen 2006) mentioned below:

1. *Hall–Petch effect (grain refinement)*: Reinforcement (fibers/particles) when introduced in a molten matrix can act as heterogeneous nucleation sites during solidification, thus giving rise to refined and equiaxed grains. When secondary processes such as hot extrusion are undertaken, grain growth during recrystallization is hindered due to the grain boundary pinning effect by the reinforcements.

2. *Orowan strengthening*: Strengthening arising due to obstacle posed by closely-spaced hard particles to the dislocation motion. Highly dispersed reinforcements significantly increase the yield strength.
3. *Enhanced dislocation density*: Usually, matrix and reinforcement materials have different CTE, due to which thermal stresses are generated during processing (e.g., during cooling in casting process). Such stress levels are large enough to increase dislocation density, especially at the matrix/reinforcement interface resulting in higher yield strengths.
4. *Load bearing effect*: Under external loads, matrix transfers the load to the reinforcement. Reinforcements have strong interfacial bonding with matrix and so good load bearing capacity is exhibited.

2.4.1 Strength Prediction

Theoretical yield strength of metal matrix composites can be estimated using the relation formulated by Nardone and Prewo (Nardone and Prewo 1986), which is based on a modified shear-lag model extended to the case of particulate composites, and is given by (2.2) as follows:

$$\sigma_{yc} = \sigma_{ym} \left\{ \left[V_p (1 + S / 2) \right] + \left[1 - V_p \right] \right\} \quad (2.1)$$

This equation takes into account the load transfer on particle from matrix, where σ_{ym} is the yield stress of unreinforced matrix, V_p is the particle volume fraction, S is the aspect ratio of particle. Equation (2.1) does not take into account, the parameters involved in strengthening of composites. Strengthening of reinforcement particles on the yield strength (σ_{ym}) of metallic matrix arises due to: (1) Orowan strengthening ($\Delta\sigma_{\text{Orowan}}$), the stress increase needed to move a dislocation through an array of impeding particles, (2) stress contribution due to statistically stored dislocations introduced by the thermal expansion mismatch between the matrix and reinforcement ($\Delta\sigma_{\text{CTE}}$), and (3) generation of geometrically necessary dislocations (GND) to accommodate the plastic deformation mismatch between the matrix and particles ($\Delta\sigma_{\text{GND}}$). When several strengthening effects are combined, the rule of addition and the root of the sum of the squares may be used to predict the yield strength, as mentioned below in (2.2). The strength of a reinforced matrix is given by,

$$\sigma_{my^1} = \sigma_{my} + \Delta\sigma \quad (2.2)$$

where σ_{my^1} and σ_{my} are the yield strength of reinforced and unreinforced matrices respectively. $\Delta\sigma$ represents the total increment in yield stress of reinforced matrix and is estimated as follows,

$$\Delta\sigma = \sqrt{(\Delta\sigma_{\text{Orowan}})^2 + (\Delta\sigma_{\text{CTE}})^2 + (\Delta\sigma_{\text{GND}})^2} \quad (2.3)$$

1. $\Delta\sigma_{\text{Orowan}}$, can be estimated using (2.4a) and (2.4b),

$$\Delta\sigma_{\text{Orowan}} = \phi \cdot \mu_m b_m / L \quad (2.4a)$$

where ϕ is a constant of order 2, μ_m and b_m are the shear modulus of metal matrix and its Burgers vector, respectively (for Al, μ_m : 26 GPa, b_m : 0.286 nm). L is the interparticle spacing of the second phase particles, which is given by

$$L = D \left(\frac{\pi}{6V_p} \right)^{1/3} \quad (2.4b)$$

where V_p and D are the volume fraction and diameter of particles, respectively.

2. $\Delta\sigma_{\text{CTE}}$ can be estimated using (2.5a) as given below:

$$\Delta\sigma_{\text{CTE}} = \eta \cdot \mu_m b_m \sqrt{\rho} \quad (2.5a)$$

where,

$$\rho = \frac{12\Delta\alpha\Delta TV_p}{b^m D(1 - V_p)} \quad (2.5b)$$

Here, η is a constant of order 1, and ρ is the dislocation density. $\Delta\alpha$ is the difference in thermal expansion coefficients between the matrix. ΔT is the temperature change from the processing temperature to room temperature.

3. $\Delta\sigma_{\text{GND}}$ is calculated using (2.6),

$$\Delta\sigma_{\text{GND}} = \beta \cdot \mu_m \sqrt{\left(\sqrt{V_p} \varepsilon^m b^m \right) / D} \quad (2.6)$$

β is a geometric factor with a numerical value ~ 0.4 , and ε_m is the plastic strain of the matrix.

2.4.2 Fracture Mechanisms

The fracture mechanisms of MMCs (such as in particulate composites) is dependent on interfacial strength and particle strength. If the interface strength is stronger than the particle strength (as in precipitation hardened composite), then the particle fracture occurs before the interface. The failure of the composite hence occurs by shear localization of fractured particles, giving rise to brittle fracture features. In short fiber composite, this type of damage gives rise to fiber cracking and fiber breakage. On the other hand, when the particle strength is higher than the interfacial strength,

it results in decohesion of particles due to void nucleation and growth in the matrix. This would be evident by ductile shear failure in the fracture surface of the composite. In short fiber composites, such a phenomenon leads to fiber pull-out in fibers that are oriented along the loading direction. Fracture also occurs by particle cracking and void formation in the matrix within clusters of particles. Particle fracture is more prevalent in coarser particles due to the following reasons: (1) the larger the particle the more it will be loaded by conventional fiber loading and end loading mechanisms and (2) coarser ceramic particles will have a higher probability of containing fracture initiating defects. Further, particle clusters give rise to a triaxial state of stress causing severe reduction in ductility resulting in catastrophic failure of the composite components.

2.5 Microstructural and Mechanical Properties of LMMCs

The attributes of Al and Mg composites are a combination of high specific stiffness, excellent wear resistance, and the potential for relatively low-cost conventional processing. Al and Mg composites have been under development for many years during which time a vast number of different types of reinforcement have been attempted with varying degrees of success. These include continuous fibers, short fibers, whiskers, and particles. Many different matrices have been tried over the years and these have a bearing on some of the properties that can be achieved in the composite. Tailoring the mechanical properties with respect to a specific application can also be achieved by varying the type and amount of reinforcement, the choice of matrix alloy, and the composite processing route. All these factors are interrelated and should not be considered in isolation when developing a new material. Among the various types of Al, Mg MMCs, the advantage of particulate reinforced composites are due to processing, wherein conventional metal manufacturing methods and machining techniques can be used (Lloyd 1994). Given that the literature available on Al and Mg composites/nanocomposites are exhaustive, only representative microstructures/mechanical data are presented here.

2.5.1 Al-Composites

Different processing methods have been used to produce various micro- and nano-reinforced Al-composites. As mentioned earlier, literature review indicates that Al_2O_3 , SiC, B_4C , BN, AlN, etc. in the form of particles/whiskers/fibers have been incorporated in various Al-matrices. Daoud and Reif (2002) studied the influence of Al_2O_3 particulates on the aging response of A356 alloy prepared using the vortex method. In these composites, the formation of MgAl_2O spinel on the interface caused depletion of Mg in the matrix, which eventually resulted in less age-hardening behavior (Fig. 2.14). The role of grain refinement treatment and the

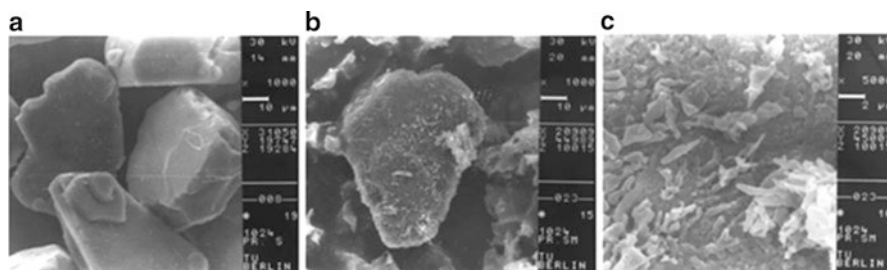


Fig. 2.14 SEM micrographs showing the morphological changes in the surface of Al_2O_3 particles in A356 alloy during melt processing (a) before addition into the molten A356 alloy (b) after addition with A356 alloy in the composite and (c) magnified view of the reaction products (*adapted from Daoud & Reif 2002*) (© 2002, Elsevier. Used with permission)

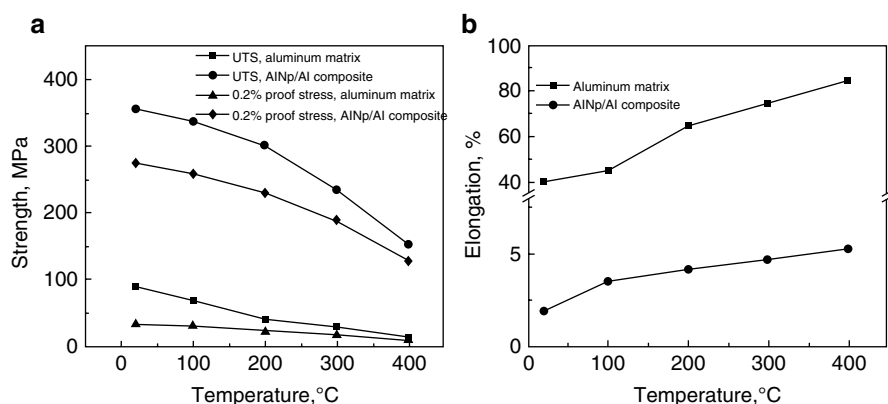


Fig. 2.15 (a, b) Room and high temperature tensile properties of Al–AlN composites. Significant improvement in (a) strength properties is achieved when compared to the unreinforced matrix, however (b) with a drastic reduction in ductility (*adapted from Zhang et al. 2003*) (© 2003, Elsevier. Used with permission)

degree of grain refinement was studied in Al-7Si-10 % V_f SiC particulate reinforced composites prepared by vortex method (Garcia-Hinojosa et al. 2004). While complete dewetting of the SiC particles and rejection from the melt was observed when K_2TiF_6 salt was used as grain refiner, the wettability improved with Al-6Ti and Al-5Ti-1B master alloy grain refiners. Significant grain refinement and uniform distribution of the reinforcement was achieved. The mechanical properties of Al–AlN composites prepared by squeeze infiltration method (Lii et al. 2002), showed that the hardness and the compressive strength increased, with a significant reduction ductility. It was identified that the crack growth path was prominent along the Al–Al, AlN–AlN, and Al–AlN interfaces. The tensile property data of Al–AlN composite showed increased yield and tensile strength, accompanied by a drastic reduction in ductility both at room and high temperatures (Fig. 2.15) (Zhang et al. 2003). Vicens et al. (2002) studied the interfacial phenomena of 2024, 6060, 5754 Al-matrices with, 45 % V_f AlN, produced by squeeze infiltration. TEM investigation

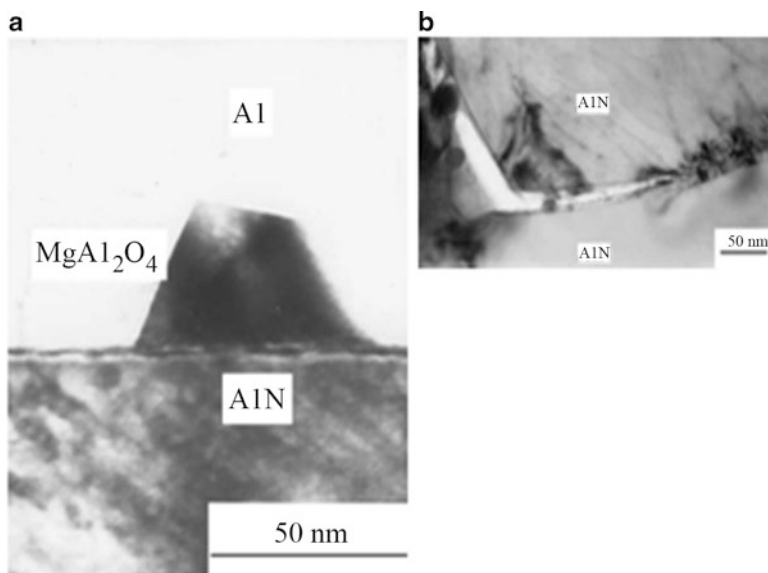


Fig. 2.16 (a) TEM image of MgAl_2O_4 precipitates formed at the interface in Al–Mg–Si/AlN composite and (b) MgO and MgAl_2O_4 interface precipitates giving rise to crack formation between two AlN grains (after compression tests) (adapted from Vicens et al. 2002) (© 2002, Elsevier. Used with permission)

revealed MgAl_2O_4 spinel crystals in 6060 and 5754 composites. In these composites, the magnesium element of the matrix reacts with a very thin alumina layer which is deposited on the AlN surfaces during the liquid infiltration step. The 5754 composite exhibited a stronger reaction leading to the formation of MgO phases with the spinel that resulted in degradation of the mechanical properties. Also, microcracking occurred mainly at the interface between two AlN grains where MgO and MgAl_2O_4 precipitated (Fig. 2.16a, b). Interfacial studies on pure Al reinforced with SiC, Al_2O_3 , and B_4C show that while an interfacial layer is formed in Al–SiC composites, none were observed in the other two composites (Shorowordi et al. 2003). However, in the Al– B_4C composite, two secondary phases consisting of carbon, aluminum, and boron were observed which based on the fracture studies give rise to a strong interface due to effective interfacial bonding.

Investigation on squeeze cast Al–Mg–BN-reinforced composites showed the formation of interfacial AlB_2 phase and in situ AlN phase which resulted in significant grain refinement (Lee et al. 2002). The interfacial reaction products of the Al/ B_4C_p composite fabricated by the pressureless infiltration method were analyzed by Lee et al. (2001) using XRD, SEM, EDS, AES, and TEM. From the SADP and CBED analysis, it was identified that AlB_2 , $\beta\text{-AlB}_{12}$ ($\text{Al}_3\text{B}_{48}\text{C}_2$), AlB_{10} ($\text{AlB}_{24}\text{C}_4$), and Al_3BC were formed as interfacial reaction products (Fig. 2.17). Similarly, interfacial study on a SiC_p /Al composite fabricated by pressureless infiltration of an Al–Mg–Si alloy into a preoxidized SiC preform confirmed the presence of MgAl_2O_4 interfacial reaction product (Fig. 2.18), which is expected to improve the wettability between the

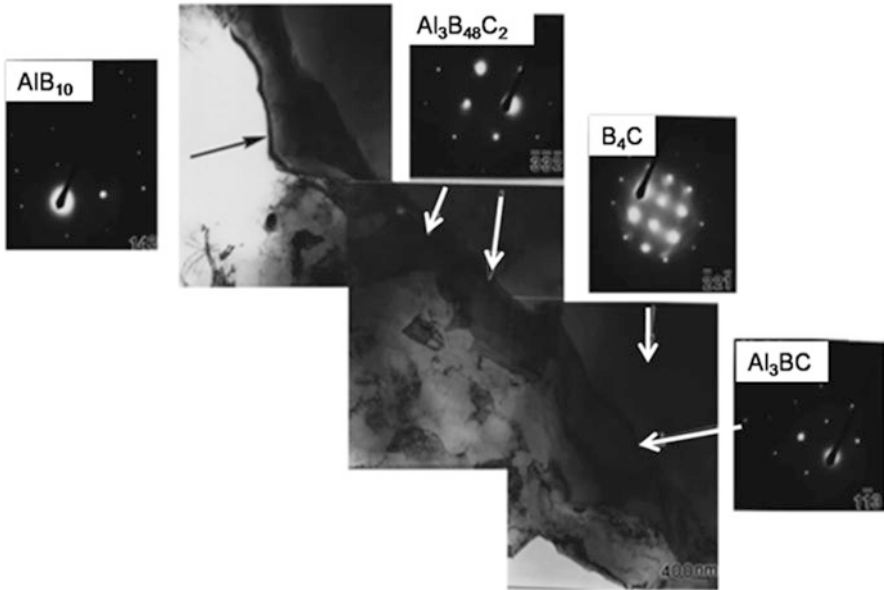
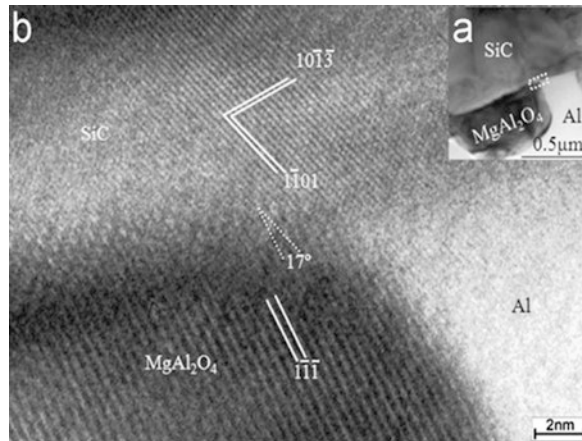


Fig. 2.17 TEM images of interfacial products between Al matrix and B_4C particles (*adapted from Lee et al. 2001*) (© 2001, Elsevier. Used with permission)

Fig. 2.18 High resolution TEM (HRTEM) image showing the formation of $MgAl_2O_4$ at the interface between Al-matrix and SiC particle. The interfacial product is expected to improve the wettability (*adapted from Zhang et al. 2013*) (© 2013, Elsevier. Used with permission)



SiC particles and the matrix (Zhang et al. 2013). The microstructure of a SiC particulate reinforced Al 2080 alloy was characterized by Evans and Boyd (2003) using focused ion beam microscopy and transmission electron microscopy. A 40 nm thick amorphous interface layer was seen to develop during processing of the composite material by diffusion of Al and Mg into the preexisting SiO_2 layer on the SiC particles. During tensile deformation, damage occurs in the near-interface zone of

the matrix, at the particle–matrix interface and within the SiC particles. TEM study of interface in Al–Si–Mg–Zn reinforced with SiC particulates prepared by pressureless infiltration method (Luo et al. 2001) showed that the reinforcement particles were coated with reaction layers of MgAl_2O_4 spinel particles, in addition to the Mg_2Si intermetallic phases found in the eutectic along the Al-grains. Tekmen et al. (2003) studied the effect of porosity on the mechanical and fracture behavior in Al–Si matrix alloy and composites reinforced with SiC particles of 10 and 20 % V_f in the as-cast state and after extrusion process. It was identified that the increase in reinforcement content increases the overall porosity content; however it reduced to low levels upon extrusion, but effective only for porosities lower than a certain size. While the increase in porosity content decreases both the yield and ultimate tensile strength value, fracture behavior was influenced by large-sized pores rather than the overall porosity content. Tee et al. (2000) investigated in situ TiB_2 particulate reinforced composites produced by the direct addition of Ti and B to molten Al, which resulted in a significant improvement in yield and tensile strengths. However, the formation of additional brittle phase (Al_3Ti flakes) during the process caused a large reduction in ductility of the in situ composite. Interfacial reaction studies on Al–TiC composites by Kennedy et al. (2001) showed the formation of large Al_3Ti precipitates in the bulk of the matrix and Al_4C_3 blocks at the particle–matrix interface.

For nanocomposites the most commonly used reinforcements are Al_2O_3 , SiC, and CNTs, while other particles such as Si_3N_4 , B_4C have also been recently considered. When nanoscale Al_2O_3 is used as the reinforcement, one major concern is its poor wettability with the Al matrix. As below 1,000 °C, the contact angle between aluminum and Al_2O_3 is greater than 90° (Schultz et al. 2011). Such poor wetting behavior results in clustering of particles, which eventually leads to deterioration in properties. In this work, Al_2O_3 nanoparticles were mixed with Mg particles so as to improve their wettability (addition of Mg increases the surface energy of nanoparticles). Hossein-Zadeh et al. (2014) studied the effect of heat treating Al_2O_3 nanoparticles prior to its addition into molten Al matrix on matrix/particle wettability. The heat treatment improved the wettability due to grooving at the grain boundary junctions, thereby improving the microstructure and mechanical properties when compared to the nanocomposite having particles without any heat treatment. Mula et al. (2009) prepared pure Al with 2 wt% nano-sized Al_2O_3 particles by ultrasonic cavitation and observed continuous nano-alumina dispersed zones near the grain boundaries in the nanocomposite. The addition of nanoparticles contributed to the significant increase in the hardness (~92 %), and tensile strength (~48 %). Su et al. (2012) reported improvements in grain refinement, ultimate tensile strength, and yield strength (37 % and 81 % respectively) but with reduction in ductility in Al-2024 nano- Al_2O_3 composite produced using casting with ultrasonic dispersion. Mazahery and Shabani (2012) prepared nano-SiC-reinforced A356 composite by compocasting and reported improvement in microstructural and mechanical properties. Xiong et al. (2011) reinforced nano-SiC particles in Al-3.0 wt % Mg matrix by pressureless infiltration and investigated the effect of SiC nanoparticles on interfacial reactions. Results showed that the formation of MgO at the interface between SiC particulates and molten Al act as a barrier for the diffusion of Si, C, and Al (Fig. 2.19), thereby improving the interfacial properties. Bathula et al. (2012)

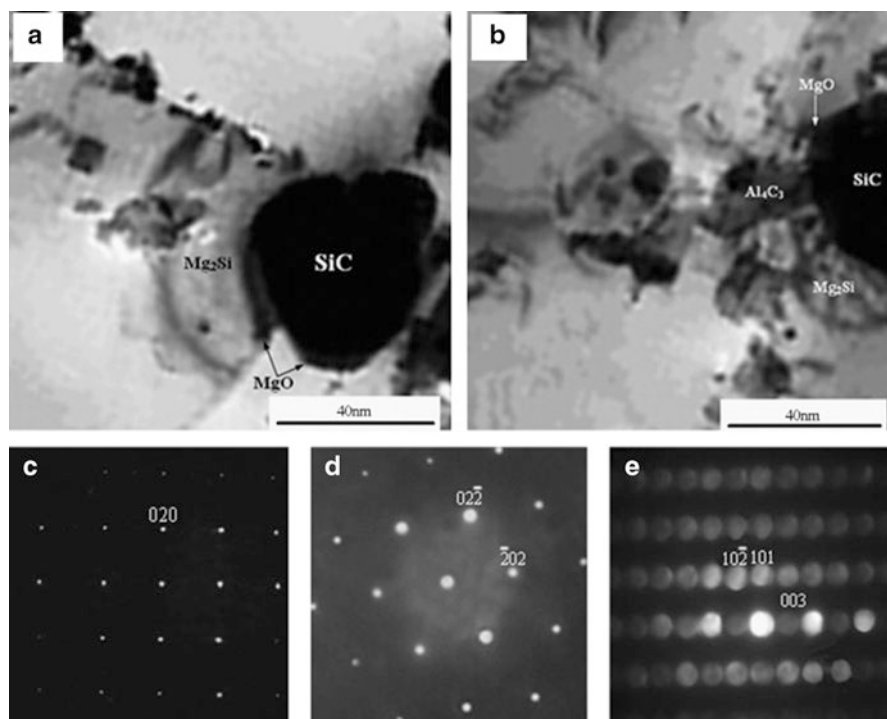


Fig. 2.19 TEM images of Al-SiC nanocomposite showing interfacial reaction products (a) TEM image of interface in composite with 10 % V_f nano SiC, (b) TEM image of interface in composite with 14% V_f nano SiC, (c) SAD pattern of Mg_2Si , (d) SAD pattern of MgO , and (e) SAD pattern of Al_4C_3 (adapted from Xiong et al. 2011) (© 2011, Elsevier. Used with permission)

synthesized Al-SiC nanocomposite with Al-5083 alloy powder and SiC nano particulates using powder metallurgy route followed by SPS. High resolution transmission microscopy (HR-TEM) analysis revealed that the matrix grain size slightly coarsened upon sintering that reduced the ductility (Fig. 2.20). Ahmed et al. (2010) prepared nanocomposites with Al-7075 alloy matrix (Al Zn-Mg Cu alloy) and nano-SiC particles and observed drastic microstructural change (i.e., grain coarsening) that caused deterioration in mechanical properties (~30 % and 40 % reduction in hardness and tensile strength, respectively). With regard to CNTs as reinforcements, the major issue that needs to be overcome is their agglomeration during processing. As an example, Esawi et al. (2010) used ball-milling to disperse up to 5 wt% CNT in Al matrix. They reported poor dispersion of CNTs (for >2 wt%) and formation of carbides in the 5 wt% sample. Liao et al. (2010) treated MWCNTs with sodium dodecyl sulfate (SDS) surfactant (as it decreases the van der Waals force between the CNTs) in order to facilitate their easy dispersion in Al-metal. They formed the Al-MWCNT composites via SPS, followed by hot extrusion. It was observed that the mechanical properties of the Al-0.5 wt% MWCNT composites

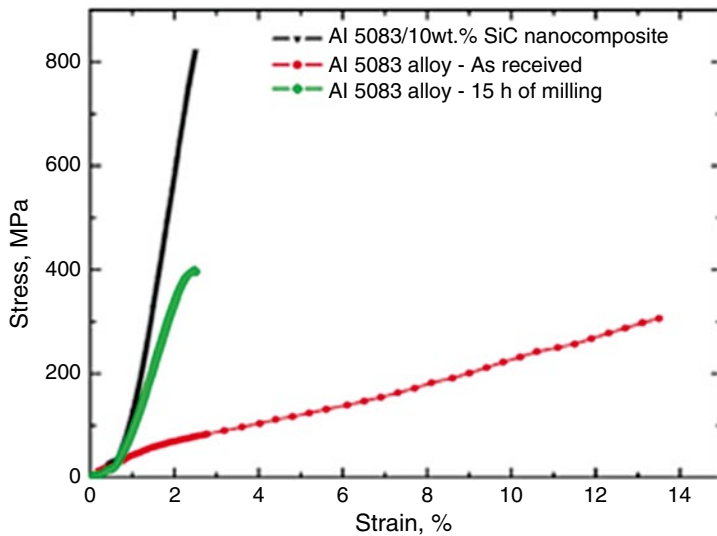


Fig. 2.20 Engineering stress–strain curves of 5083 Al-alloy in the as-received, milled (nanostructured), and nano-reinforced condition. Note the large improvement in strength due to nano-reinforcement addition, with little or no ductility (*adapted from Bathula et al. 2012*) (© 2012, Elsevier. Used with permission)

enhanced noticeably (in both tension and compression). Any increase in wt % of CNTs thereafter decreased the mechanical properties due to agglomeration and insufficient interfacial bonding. The mechanical properties of selected Al-micro/nanocomposites are listed in Table 2.5.

2.5.2 Mg Composites

Mg, unlike Al has h.c.p. structure and possesses limited number of slip systems. Its deformation behavior is governed by both slip and twinning (Dieter 1988). The strengthening mechanisms in Mg materials are strongly influenced by their texture, i.e., preferred crystallographic orientation. Texture evolution is influenced by the form in which the material exists (cast or wrought form), i.e., while casting can give rise to random crystallographic orientation and hence isotropic properties, wrought materials (strong orientation of crystallographic planes) give rise to anisotropic deformation behavior (Wang and Huang 2003). Further, slip/twinning deformation modes are determined by the direction of loading. For instance, in extruded Mg materials, the basal planes are aligned strongly in the extrusion direction, which are highly unfavorable for the basal slip to occur. Due to this reason, the tensile ductility of extruded Mg materials is limited/lower when the testing is carried out in the direction parallel to the extrusion direction (Reed-Hill 1973; Wang and Huang

Table 2.5 Mechanical properties of several Al-metal matrix composites/nanocomposites

Material	Microhardness (Hv)	Yield strength (MPa)	Ultimate strength (MPa)	% Ductility	Elastic modulus (GPa)
Al-Si (Lloyd 1994)					
A356 (T6)	–	205	280	6	76
A356-10%SiCp (T61)	–	287	308	0.5	82
A356-15%SiCp (T61)	–	329	336	0.2	91
A356-20%SiCp (T61)	–	336	357	0.4	98
A380 (F)	–	160	320	3.7	72
A380-10%SiCp (F)	–	245	332	1.0	9.5
A380-20%SiCp (F)	–	308	356	0.4	114
Al-Mg-Si (Lloyd 1994)					
6061 (T6)	–	275	310	20	69
6061-10 %Al ₂ O ₃ p (T6)	–	296	338	7.8	81
6061-15 %Al ₂ O ₃ p (T6)	–	317	359	7.4	87
6061-20 %Al ₂ O ₃ p (T6)	–	359	379	2.1	98
6061-15 %SiCp (T6)	–	342	364	3.2	91
6061-15 % SiCp (T4)	–	405	460	7.0	98
6061-20 % SiCp (T4)	–	420	500	5.0	1.5
6061-25 % SiCp (T4)	–	430	515	4.0	115
Al-Cu (Lloyd 1994)					
2014 (T6)	–	476	524	13	73
2014-10 %Al ₂ O ₃ p (T6)	–	483	517	3.3	84
2014-15 %Al ₂ O ₃ p (T6)	–	476	503	3.2	92
2014-20 %Al ₂ O ₃ p (T6)	–	483	503	1.0	101
2014-15 %SiCp (T6)	–	466	493	2.0	100
2124 (T6)	–	325	472	12	72
2124-17.8 %SiCp (T4)	–	400	610	5–7	100
2124-25 % SiCp (T4)	–	490	630	2–4	116
2124-20 % SiCp (T4)	–	4.5	560	7	105
Al-Zn-Mg (Lloyd 1994)					
7075 (T6)	–	505	570	10	72
7075-15 % SiCp (T651)	–	556	601	3	95
7049-15 % SiCp (T6)	–	598	643	2	90
7090-20 % SiCp (T6)	–	665	735	2	105
Al-Li (Lloyd 1994)					
8090 (T6)	–	415	485	7	90
8090-13 %SiCp (T4)	–	454	520	5	101
8090-13 % SiCp (T6)	–	499	547	3	101
8090-17 % SiCp (T4)	–	310	460	4–7	103
8090-17 % SiCp (T6)	–	450	540	3–4	103

(continued)

Table 2.5 (continued)

Material	Microhardness (Hv)	Yield strength (MPa)	Ultimate strength (MPa)	% Ductility	Elastic modulus (GPa)
Lii et al. (2002)					
Al-51 % AlN	92	—	—	—	—
Al-60 % AlN	120	—	—	—	—
Al-63 % AlN	130	—	—	—	—
Al-70 % AlN	150	—	—	—	—
<i>Nanocomposites</i>					
Hossein-Zadeh et al. (2014)					
A356 (C)	53.2	75	213	22	—
A356+1.0 wt% nAl ₂ O ₃ (non-HT) (C)	63.4	125	265	42	—
A356+1.0 wt% nAl ₂ O ₃ (HT) (C)	70.6	180	375	48	—
Mula et al. (2009)					
Al (conventional cast) (T)	36	30	62	47	—
Al (USC) (T)	51	47	92	36	—
Al+2 % nAl ₂ O ₃ (USC+CR) ratio 1.1	118	—	—	—	—
Al+2 % nAl ₂ O ₃ (USC+CR) ratio 2.0	139	—	—	—	—
Su et al. (2012)					
AA2024 (USC) (T)	—	83	154	1.4	—
AA2024+0.5 wt% nAl ₂ O ₃ (USC) (T)	—	139	194	1.2	—
AA2024+1 wt% nAl ₂ O ₃ (USC) (T)	—	154	212	1	—
AA2024+1.5 wt% nAl ₂ O ₃ (USC) (T)	—	149	208	0.6	—
AA2024+2 wt% nAl ₂ O ₃ (USC) (T)	—	144	203	0.5	—
Mazahery and Shabani (2012)					
A356 (SC) (T)	HB				
A356 (CC) (T)	52	122	147	6.0	—
A356+0.5 % V _f nSiC (SC) (T)	55	130	157	8.0	—
A356+0.5 % V _f nSiC (CC) (T)	64	127	227	3.8	—
A356+0.5 % V _f nSiC (CC) (T)	65	138	243	5.6	—
A356+1.5 % V _f nSiC (SC) (T)	67	135	240	3.7	—
A356+1.5 % V _f nSiC (CC) (T)	70	143	253	5.0	—

(continued)

Table 2.5 (continued)

Material	Microhardness (Hv)	Yield strength (MPa)	Ultimate strength (MPa)	% Ductility	Elastic modulus (GPa)
A356+2.5 % V_f nSiC (SC) (T)	73	143	260	3.7	–
A356+2.5 % V_f nSiC (CC) (T)	75	147	273	4.5	–
A356+3.5 % V_f nSiC (SC) (T)	76	146	290	3.6	–
A356+3.5 % V_f nSiC (CC) (T)	80	149	295	4.3	–
A356+4.5 % V_f nSiC (SC) (T)	75	138	247	3.3	–
A356+4.5 % V_f nSiC(CC) (T)	82	151	303	4.1	–
Bathula et al. (2012)					
Al5083 (unmilled) (C)	148	–	280	13.8	–
Al5083 (milled) (C)	250	–	400	3.12	–
Al5083 + 10 wt% nSiC (milled + SPS) (C)		–	824	2.5	–
Esawi et al. (2010)					
Al (T)	–	–	170	–	–
Al+0.5 wt% CNT (ball-mill+hot ext.) (T)	–	–	220	–	–
Al+1.0 wt% CNT (ball-mill+hot ext.) (T)	–	–	240	–	–
Al+2.0 wt% CNT (ball-mill+hot ext.) (T)	–	–	255	–	–
Al+5.0 wt% CNT (ball-mill+hot ext.) (T)	–	–	250	–	–

2003) giving rise to large difference between tensile and compression yield strengths (tension-compression yield asymmetry). Favorable orientations of crystallographic planes can give rise to better properties in terms of both strength and ductility, and can be obtained by varying the alloying additions, reinforcement incorporation, and heat treatments/precipitation.

Mg composites are usually reinforced with SiC and Alumina in the form of fibers/whiskers/particulates. Some studies also use carbon fibers; however carbon has poor wetting characteristics with Mg, and in the absence of surface modification of the fiber it results in interface debonding, and is ineffective as reinforcement. Hu et al. (2010) investigated the influence of interfacial properties on the mechanical and in situ fracture behavior of saffil alumina short-fiber-reinforced AE44 (Mg–4.0Al–4.1RE–0.3Mn) composite. Interfacial studies indicated that the SiO_2 binder in the preform reacted with molten Mg during infiltration and formed MgO. Further, lamellar and particle intermetallic phases composed of Al–RE

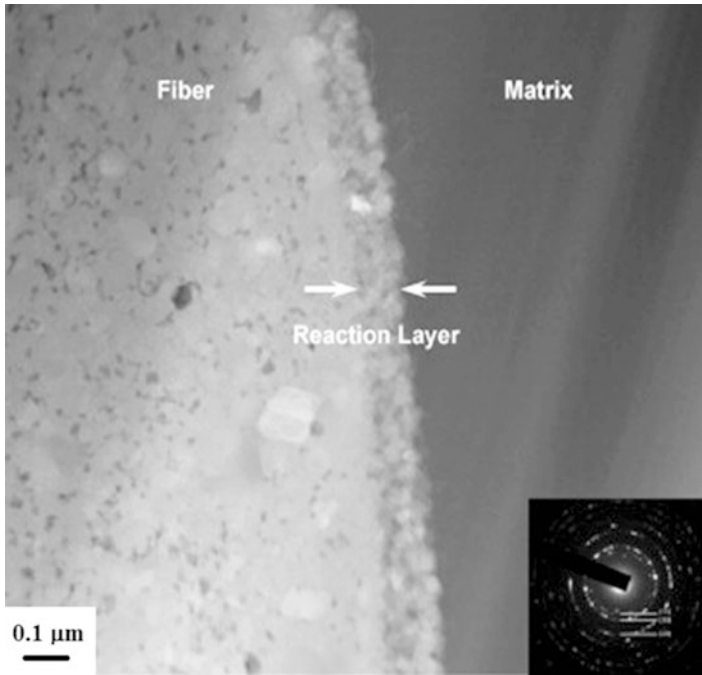


Fig. 2.21 Formation of interfacial MgO layer in AE44/Saffil Al_2O_3 fiber-reinforced composites (adapted from Hu et al. 2010) (© 2010, Elsevier. Used with permission)

($\text{Al}_{11}\text{RE}_3$ and Al_2RE) were formed on the fiber surface as well as in the matrix. While there was an increase in the elastic modulus, yield, and tensile strengths, a large reduction in ductility ($\sim 10\%$ in unreinforced alloy reduced to $\sim 1\%$ in the composite) was reported. Fracture studies showed that microcracks initiated in the region of interface leading to interfacial debonding and/or fiber breakage (Fig. 2.21). Contreras (2004) prepared high volume fraction in situ TiC/AZ91D composites using infiltration technique. The room and high temperature tensile properties indicated improved strengthening due to reinforcement but with a loss in ductility (brittle characteristics). Hu and Wang (2000) prepared ZK51/SiCw reinforced composites by a two-step squeeze infiltration process. Their study revealed that the casting temperature determines the interfacial characteristics/reactions and hence the final properties. While a lower casting temperature caused interfacial debonding, a higher casting temperature resulted in melt oxidation and grain coarsening.

Microstructure and interface studies of $\text{Mg}_2\text{B}_2\text{O}_5$ whisker reinforced AZ91D composite by Chen et al. (2010) showed that the $\text{Mg}_2\text{B}_2\text{O}_5$ whiskers have a twinned structure with the (2 0 2) as the twin plane and growth direction along [0 1 0] and that MgB_4O_7 particles and globular Mg_2Si particles were observed within the $\text{Mg}_2\text{B}_2\text{O}_5$ whisker, and $\text{Mg}_2\text{B}_2\text{O}_5$ whiskers/Mg-matrix interface. Further, MgO and MgB_2 phase formed at the matrix-whisker interface during vacuum–gas pressure infiltration process due to the interfacial reaction (Fig. 2.22). Further the rough and uneven interfacial layer would have negative effect on the interfacial bonding. The

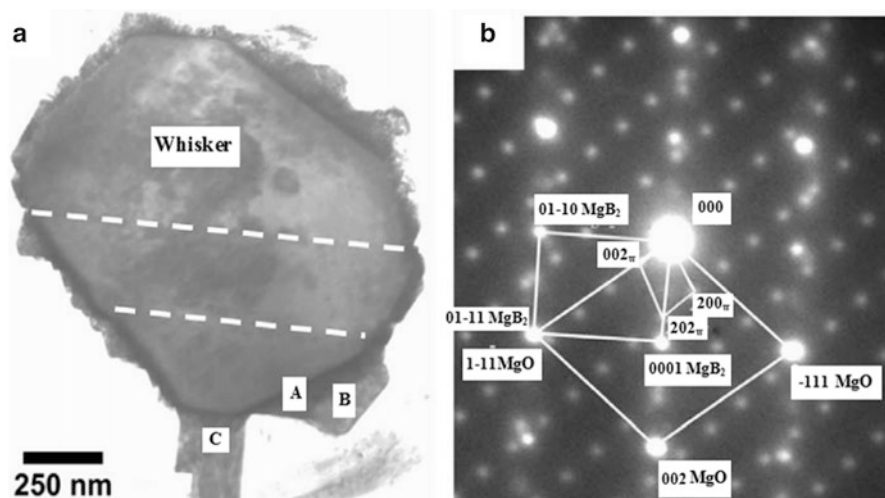


Fig. 2.22 TEM image showing the existence of two interfacial layers in $\text{Mg}_2\text{B}_2\text{O}_5$ whisker reinforced Mg composite (a) TEM BF image of $\text{Mg}_2\text{B}_2\text{O}_5$ whisker. Two dash lines delineate the trace of the twin planes; (b) SAED pattern of the $\text{Mg}_2\text{B}_2\text{O}_5$ whisker along $[010]$ $\text{Mg}_2\text{B}_2\text{O}_5$, $[1\ 1\ 0]$ MgO and $[2\text{-}1\text{-}10]$ MgB_2 zone axes detected at the connection area of position C (adapted from Chen et al. 2010) (© 2010, Elsevier. Used with permission)

mechanical properties indicate a dramatic increase of modulus, yield, and tensile strengths in the composite when compared to that of the AZ91D cast alloy, however, at the expense of ductility (large reduction in % elongation). Similar increase in strength and drastic reduction in ductility was observed in hybrid Mg-composite with SiC particles and mullite fibers (Gu et al. 2004). Comparatively, in Mg-hydroxyapatite (HA) composite, not much improvement in strength was observed, but ductility reduced significantly (Gu et al. 2010). Wang et al. (2006) produced Mg–Li matrix composite with 5 wt% Al_2Y particulates by stir casting technique and identified homogenous distribution of Al_2Y intermetallics particles in the matrix, along with a stable interface with no reaction products. Mechanical properties showed better hardness, modulus, and tensile strength, with ~42 % reduction in ductility. Similar behavior was observed in stir cast Mg–Zn–Ca/SiCp reinforced composites (Fig. 2.23) (Wang et al. 2012) and squeeze infiltrated ZK60A/(SiCw + B_4Cp) reinforced hybrid composites (Zhang et al. 1997). The effect of high temperature exposure on the interface and tensile properties of AZ91/ $\text{Al}_{18}\text{B}_4\text{O}_{33}\text{w}$ composite fabricated by squeeze casting was studied by Zheng et al. (2004). It was identified that the interfacial region was composed of MgO (10–20 nm thick), which prevented the formation of reaction products between the whisker and the matrix. Improvement in elastic modulus and strength properties was observed with an inevitable drastic reduction in ductility. The effect of acid aluminum phosphate binder was reported in AZ91/SiCw composites fabricated by squeeze casting process (Zheng et al. 2001). For the composites with no binders, the SiC_w-AZ91 interfaces are very clean, whereas for the composites

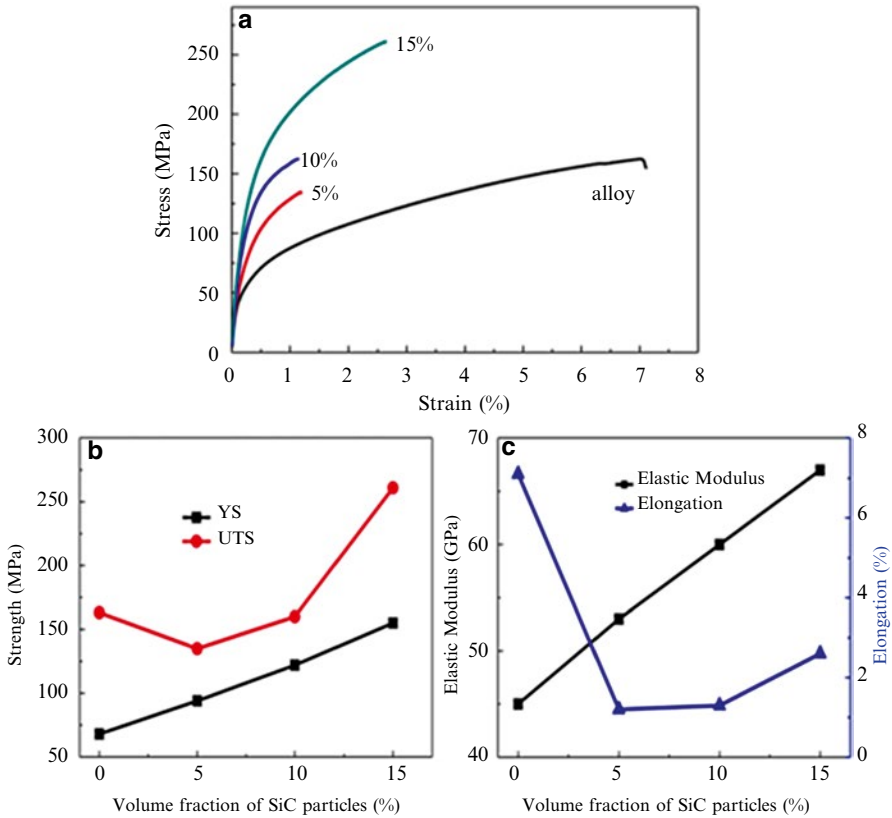


Fig. 2.23 (a) stress–strain curves (b) effect of volume fraction on strength and (c) effect of volume fraction on elongation in Mg–Zn–Ca/SiC particulate reinforced composites. Note that the variation in properties is influenced by the volume fraction, and that the ductility decreases drastically in the composites (*adapted from Wang et al. 2012*) (© 2012, Elsevier. Used with permission)

with acid phosphate binders, fine, uniform, and discrete interfacial MgO reaction products at the interface exist due to reaction between the binder and molten Mg (Fig. 2.24). The definite crystallographic orientation relationship between MgO and SiCw lead to a compatible interface with good lattice matching, and increase whisker–matrix interfacial bonding strength. Due to efficient load transfer from the matrix to whisker, improved modulus and tensile strength of the composites are achieved, at the expense of ductility. Jayalakshmi et al. studied the mechanical behavior of Al_2O_3 short-fiber-reinforced composites with two different matrices, AM100 alloy and ZC63 alloy (Jayalakshmi et al. 2002, 2006). It was identified that the composites show no or little improvement in strength at room temperature along with a large reduction in ductility. Further, the properties at high temperatures showed that the tensile behavior was not dependent on temperature and volume fraction, and that they were influenced by the nature of the base matrix (i.e., brittle/ductile).

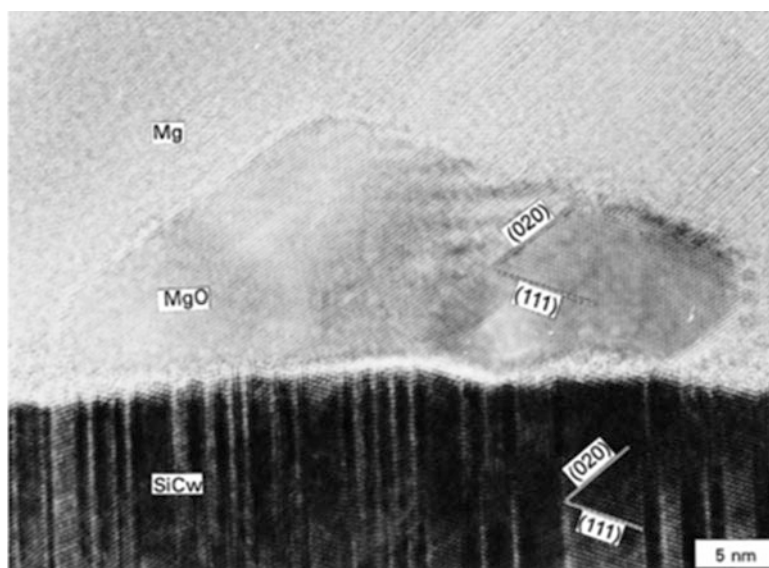


Fig. 2.24 Interfacial reaction resulting in the formation of MgO in AZ91/SiC-whisker reinforced composite with $\text{Al}(\text{PO}_3)_3$ binder (adapted from Zheng et al. 2001) (© 2001, Elsevier. Used with permission)

Considering nanoscale reinforcements, nano- Al_2O_3 has limited reactivity with molten Mg and therefore Mg- Al_2O_3 nanocomposites were the first of the Mg MMNCs to be prepared. Hassan and Gupta (2005) synthesized pure Mg-based nanocomposite with 1.1 V_f (%) of Al_2O_3 particulates (size 50 nm) using DMD technique, followed by hot extrusion. The tensile properties showed an increase in yield strength by ~90 % and increase in ductility by ~45 %, when compared to the unreinforced Mg. In AZ31B-1.5 % V_f Al_2O_3 nanocomposites produced by DMD, Nguyen and Gupta (2008) observed near-equiaxed grains with decreasing grain size, and roundness of second phase with increasing nano- Al_2O_3 content. Tensile properties (assessed in terms of work of fracture) improved more than four times with enhanced ductility. CNTs have been used in Mg matrices to make composites. Goh et al. (2006) fabricated Mg nanocomposites containing 0.3, 1.3, 1.6, and 2 wt% CNTs using DMD process, that were hot extruded and characterized for their material behavior. TEM investigations (Goh et al. 2008) of dislocation structures in pure Mg and Mg 1.3CNT nanocomposites (Figs. 2.25 and 2.26) showed that only basal dislocations were present in pure Mg (no prismatic or pyramidal slip planes), whereas in Mg 1.3 wt% CNT nanocomposite, basal and prismatic slip planes were observed. Additional slip systems observed in the CNT-reinforced nanocomposites showed the propensity of nano-reinforcement addition in activating the nonbasal slip systems, which strongly influence the mechanical behavior. Mg matrices have been incorporated with SiC nanoparticles by various methods. Microstructural analyses of the as-cast specimens of pure Mg nanocomposites reinforced with 2 wt% nano-SiC

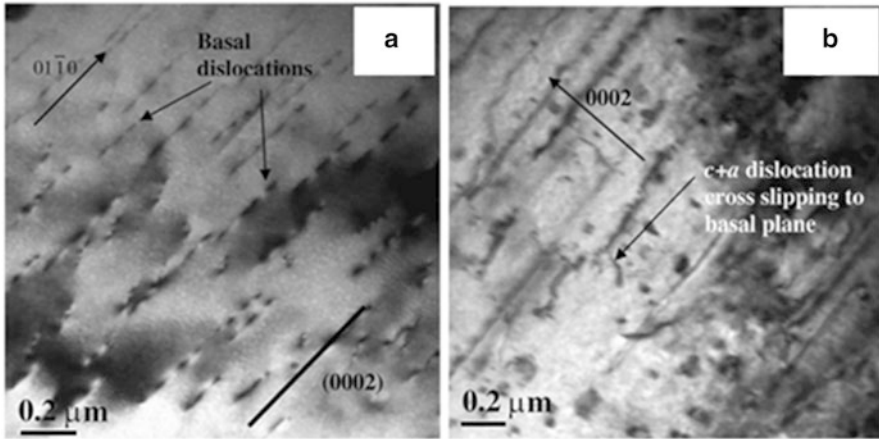


Fig. 2.25 TEM investigation on pure Mg produced by the DMD method. The images show the dislocation structures on: (a) (2-1-10) foil plane and (b) (2-1-10) foil plane. Basal plane trace common to (a) and (b) is indicated by white line (adapted from Goh et al. 2008) (© 2008, Elsevier. Used with permission)

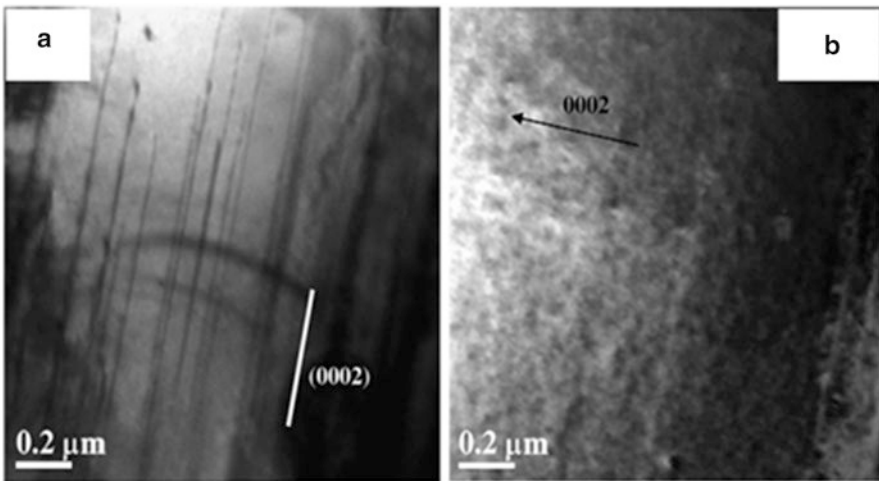


Fig. 2.26 TEM images of dislocation structures in Mg-1.3 wt% CNT nanocomposite observed on: (a) (2-1-10) foil plane and (b) (2-1-10) foil plane. Basal plane trace common to (a) and (b) is indicated by black line. The composite was produced using the DMD method (adapted from Goh et al. 2008) (© 2008, Elsevier. Used with permission)

particles by ultrasonic cavitation-based dispersion method (Erman et al. 2012) showed about 60 % reduction in grain size of the composite. Mg-(2-4)Al-1SiC with 2 % nano-SiC by ultrasonic cavitation method (Cao et al. 2008) showed good dispersion of nanoparticles (embedded inside the grains) with good interface bonding (no intermetallic phase formation). The yield strength of the Mg-2Al-1Si-2%SiC

and Mg-4Al-1Si-2%SiC nanocomposites improved significantly, while retaining the ductility. AZ63 reinforced with nano-SiC particles (size 40 nm) using FSP (Sun et al. 2012) showed no interfacial reaction products at the matrix/particle interface. The ultimate tensile strength of the composite increased significantly (~312 MPa) when compared to ~160 MPa of the unreinforced alloy. Other representative studies that investigate nanocomposites properties are given in refs. Paramsothy et al. (2009, 2010), Jayaramanavar et al. (2009), Nguyen and Gupta (2010), Sankaranarayanan et al. (2011), Thakur et al. (2007a, b, c), Tun et al. (2012). The mechanical properties of selected Mg-micro/nanocomposites are listed in Table 2.6.

Table 2.6 Mechanical properties of several Mg-metal matrix composites/nanocomposites

Material	Microhardness (Hv)	Yield strength (MPa)	Ultimate strength (MPa)	% Ductility	Elastic modulus (GPa)
Hu et al. (2010)					
AE44 (infiltration)	–	98.05	197.69	10.26	43.6
AE44-15 % V_f Al ₂ O ₃ (infiltration)	–	163.26	221.62	1.28	72.3
Lloyd (1994)					
AZ61 (cast)	–	157	198	3	38
AZ61-20 % V_f SiC (cast)	–	260	328	2.5	47.5
AZ91 (cast)	–	168	311	21	49
AZ91-9.4 % V_f SiC (cast)	–	191	276	2	47.5
AZ91-15.1 % V_f SiC (cast)	–	260	328	2.5	80
Contreras (2004)					
Mg-56 % V_f TiC (pressureless infiltration)	195	–	200	–	130
Chen et al. (2010)					
AZ91D (vacuum–gas pressure infiltration)	–	97	165	7.3	45
AZ91D-50 % V_f Mg ₂ B ₂ O ₅	–	262	265	0.98	54
Gu et al. (2004)					
Pure Mg (liquid pressure infiltration)	–	–	98	16	–
Mg-8 % V_f (SiCp-Al ₂ O ₃ -SiO ₂ -f)	–	–	210	2.13	–
Mg-18 % V_f (SiCp-Al ₂ O ₃ -SiO ₂ -f)	–	–	267	0.64	–

(continued)

Table 2.6 (continued)

Material	Microhardness (Hv)	Yield strength (MPa)	Ultimate strength (MPa)	% Ductility	Elastic modulus (GPa)
Gu et al. (2010)					
Pure Mg (PM + Ext)	–	107	197	10.3	–
Mg-10 wt% HA (PM + Ext)	–	117	171	6.7	–
Mg-20 wt% HA (PM + Ext)	–	105	146	4.3	–
Mg-30 wt% HA (PM + Ext)	–	71	92	2.6	–
Wang et al. (2006)					
Mg–Li (As-cast)	–	67.9	130	12	34.6
Mg-5 wt%Al ₂ Y (As-cast)	–	107.4	189	7	50.1
Zhang et al. (1997)					
ZK60A (liquid pressure infiltration)	–	–	315	10.4	42.2
ZK60A-24 % V _f (SiCw-B ₄ Cp)	–	–	428	2.3	80.6
Zheng et al. (2004)					
AZ91 (As-cast)	–	90	188	11.72	45
AZ91-Al ₁₈ B ₄ O ₃₃ w (As-cast)	–	266	352	0.97	67
AZ91-Al ₁₈ B ₄ O ₃₃ w (250 °C/100 h) _z	–	270	368	0.96	71
AZ91-Al ₁₈ B ₄ O ₃₃ w (400 °C/50 h)	–	261	353	0.96	65
Zheng et al. 2001)					
AZ91 (squeeze cast)	54	87	189	8.14	45
AZ91-20 % V _f SiCw (Al(PO ₃) ₃ binder)	175	220	355	1.38	85
AZ91-20 % V _f SiCw (without binder)	174	202	314	1.29	77
Jayalakshmi et al. (2002)					
AM100 (T6) squeeze infiltration	86	–	230	2	46
AM100-15% V _f Al ₂ O _{3-SF} (T6) (SI)	145	–	220	1.5	69
AM100-20% V _f Al ₂ O _{3-SF} (T6) (SI)	156	–	220	0.9	76
AM100-25% V _f Al ₂ O _{3-SF} (T6) (SI)	163	–	218	0.43	85
Jayalakshmi et al. (2006)					
ZC63 (T6) squeeze infiltration (SI)	60	195	270	8.2	47

(continued)

Table 2.6 (continued)

Material	Microhardness (Hv)	Yield strength (MPa)	Ultimate strength (MPa)	% Ductility	Elastic modulus (GPa)
ZC63-15 % V_f Al_2O_{3-SF} (T6) (SI)	115	202	210	0.55	72
ZC63-20% V_f Al_2O_{3-SF} (T6) (SI)	138	202	212	0.73	80
ZC63-25% V_f Al_2O_{3-SF} (T6) (SI)	144	140	150	0.62	88
<i>Nanocomposites</i>					
Hassan and Gupta (2005)					
Pure Mg (DMD + hot ext.)	40	97	173	7.4	–
Mg + 1.1 % V_f nAl_2O_3 (DMD + hot ext.)	65	175	246	14	–
Nguyen and Gupta (2008)					
AZ31B (DMD + hot ext.)	63	201	270	5.6	–
AZ31B + 1.5 % V_f nAl_2O_3 (DMD + hot ext.)	86	144	214	29.5	–
Jayaramanavar et al. (2009)					
ZK60A (DMD + hot ext.) (T)	97	139 ± 4	246 ± 4	20.2 ± 2	–
ZK60A + 1.5 % V_f nAl_2O_3 (DMD + hot ext.) (T)	92	147 ± 8	252 ± 5	26.0 ± 1	–
Paramsothy et al. (2009)					
AZ31 (DMD + hot ext.) (T)	64	172 ± 15	263 ± 12	10.4 ± 3.9	–
AZ31 + 1.5 % V_f nAl_2O_3 (DMD + hot ext.) (T)	83	204 ± 10	317 ± 5	22.2 ± 2.4	–
Sankaranarayanan et al. (2011)					
Mg (DMD + hot ext.) (T)	48	125 ± 9	169 ± 11	6.2 ± 0.7	–
Mg 5.6 Ti-2.5 % nAl_2O_3 (wt. %) (DMD) (T)	74	175 ± 4	227 ± 10	3.3 ± 0.2	–
Mg 5.6 Ti-2.5 % nAl_2O_3 (BM) (DMD) (T)	69	168 ± 8	214 ± 8	6.8 ± 0.8	–
Paramsothy et al. (2010)					
AZ31 (DMD + hot ext.) (T)	64	172 ± 15	263 ± 12	10.4 ± 3.9	–
AZ31 + 1 % V_f CNT (DMD + hot ext.) (T)	95	190 ± 13	307 ± 10	18.0 ± 2.6	–
Nguyen and Gupta (2008)					
AZ31B (DMD + hot ext.) (T)	63	201 ± 7	270 ± 6	5.6 ± 1.4	–

(continued)

Table 2.6 (continued)

Material	Microhardness (Hv)	Yield strength (MPa)	Ultimate strength (MPa)	% Ductility	Elastic modulus (GPa)
AZ31B + 1.5 V_f nAl ₂ O ₃ + 3Ca (DMD) (T)	113	235 ± 7	285 ± 14	7.3 ± 0.2	–
Tun et al. (2012)					
Mg (microwave sint.) (MWS + hot ext.) (T)	45	121 ± 5	179 ± 6	11 ± 1	–
Mg 1.0 V_f nZnO(MWS + hot ext.) (T)	62	125 ± 4	231 ± 13	17 ± 2	–
Thakur et al. (2007a)					
Mg (MWS + hot ext.) (T)	39	119 ± 7	170 ± 4	5.4 ± 1.5	–
Mg 1.0 nSiC(MWS + hot ext.) (T)	43	131 ± 12	182 ± 9	5 ± 0.4	–
Mg 0.5 nSiC + 0.5 nAl ₂ O ₃ (MWS + hot ext.) (T)	46	155 ± 7	197 ± 1	4.6 ± 2	–
Thakur et al. (2007c)					
Mg 1.0 CNT(MWS hot ext.) (T)	43	113 ± 2.8	146 ± 6.5	1.9 ± 0.9	–
Mg + 0.3 CNT-0.7 nAl ₂ O ₃ (MWS) (T)	44	153 ± 2.1	196 ± 3.3	2.5 ± 0.8	–
Thakur et al. (2007b)					
Mg (MWS hot ext.) (T)	41	112 ± 7.7	155 ± 2.1	5.9 ± 1.2	–
Mg 1.0 CNT (MWS hot ext.) (T)	43	117 ± 6.2	153 ± 2.8	1.5 ± 0.3	–
Mg 0.5 CNT + 0.5 nSiC(MWS) (T)	45	152 ± 1.2	188 ± 2.7	2.3 ± 0.6	–
Erman et al. (2012)					
Mg (USC)	–	47	120	12.3	–
Mg-1 wt% nSiC (USC)	–	67	133	6.3	–
Cao et al. (2008)					
Mg (2,4)Al 1Si (USC) (T)	–	62	145	8.8	–
Mg (2,4)Al 1Si-2 nSiC (USC) (T)	–	82	178	9.5	–
Sun et al. (2012)					
AZ63 (FSP) (T)	80	–	150	6	–
AZ63-nSiC (FSP) (T)	110	–	300	11	–

2.6 Limitations

In spite of the various advantages that the conventional ceramic reinforced LMMCs can provide, there exists a critical limitation that has restricted their application potential—which is their low ductility. As seen from Tables 2.5 and 2.6, the tensile elongation decreases rapidly with the addition of reinforcing particles. The reduction in ductility arises due to the inherent brittle nature of the reinforcement and the poor interfacial characteristics between the reinforcement/matrix. Poor interface occurs because of the low wettability between the matrix and the particles/binder or reactions between binder/particle and the matrix. Owing to this drawback, particle decohesion, particle agglomeration/clusters, and nonbeneficial interfacial reactions occur. As mentioned earlier in Sect. 2.4.2, fracture behavior of composite is associated with the interfacial strength or lack thereof.

In this context, there lies a great demand to explore better alternative reinforcements. The most promising solution is to incorporate bulk metallic glasses (BMG) as replacements for conventional ceramic reinforcements. BMGs are new class of metallic materials that exhibit superior mechanical properties, due to their structural properties (absence of long-range atomic order) and thermal behavior (i.e., existence of glass-transition, T_g , and crystallization temperature, T_x). With these unique properties, amorphous alloys exhibit high strength ($\sim 1\text{--}2$ GPa) and large elastic strain limit ($\sim 1\text{--}2$ %). When these novel materials are used as reinforcements in LMMCs, they can provide excellent interfacial properties and impart superior strength due to them being metallic in nature (metallic bonding), when compared to conventional ceramic reinforcements (covalent/ionic bonds). This will invoke synergistic effect of the inherent structural/mechanical/thermal properties of the matrix and reinforcements, in order to achieve superior performance of LMMCs.

References

- Abbasipour B, Niroumand B, Monir Vaghefi SM (2010) Compcasting of A356-CNT composite. *Trans Nonferrous Met Soc China* 20:1561–1566. doi:[10.1016/S1003-6326\(09\)60339-3](https://doi.org/10.1016/S1003-6326(09)60339-3)
- Abramov O (1994) *Ultrasound in liquid and solid metals*. CRC Press, Boca Raton
- Ahmed A, Neely AJ, Shankar K et al (2010) Synthesis, tensile testing, and microstructural characterization of nanometric SiC particulate-reinforced Al 7075 matrix composites. *Metall Mater Trans A* 41:1582–1591. doi:[10.1007/s11661-010-0201-y](https://doi.org/10.1007/s11661-010-0201-y)
- Arsenault R (1983) Particulate microstructure of fiber and SiC in 6061 Al composites. *Scr Metall* 17:67–71
- Balog M, Yu P, Qian M et al (2013) Nanoscaled Al–AlN composites consolidated by equal channel angular pressing (ECAP) of partially in situ nitrated Al powder. *Mater Sci Eng A* 562:190–195
- Bathula S, Anandani RC, Dhar A, Srivastava K (2012) Microstructural features and mechanical properties of Al 5083/SiCp metal matrix nanocomposites produced by high energy ball milling and spark plasma sintering. *Mater Sci Eng A* 545:97–102. doi:[10.1016/j.msea.2012.02.095](https://doi.org/10.1016/j.msea.2012.02.095)
- Brown L, Stobbs W (2006) The work-hardening of copper-silica v. equilibrium plastic relaxation by secondary dislocations. *Philos Mag* 34:351–372

- Cao G, Konishi H, Li X (2008) Mechanical properties and microstructure of SiC-reinforced Mg-(2,4)Al-1Si nanocomposites fabricated by ultrasonic cavitation based solidification processing. *Mater Sci Eng A* 486:357–362. doi:[10.1016/j.msea.2007.09.054](https://doi.org/10.1016/j.msea.2007.09.054)
- Chawla N, Chawla K (2006) Metal matrix composites. Springer, New York
- Chawla K, Metzger M (1978) Advances in research on strength and fracture of materials, vol 3. Pergamon Press, New York, p 1039
- Chen SH, Jin PP, Schumacher G, Wanderka N (2010) Microstructure and interface characterization of a cast $\text{Mg}_2\text{B}_2\text{O}_5$ whisker reinforced AZ91D magnesium alloy composite. *Compos Sci Technol* 70:123–129. doi:[10.1016/j.compscitech.2009.09.015](https://doi.org/10.1016/j.compscitech.2009.09.015)
- Contreras A (2004) Mg/TiC composites manufactured by pressureless melt infiltration. *Scr Mater* 51:249–253. doi:[10.1016/j.scriptamat.2004.04.007](https://doi.org/10.1016/j.scriptamat.2004.04.007)
- Daoud A, Reif W (2002) Influence of Al_2O_3 particulate on the aging response of A356 Al-based composites. *J Mater Process Technol* 123:313–318. doi:[10.1016/S0924-0136\(02\)00103-6](https://doi.org/10.1016/S0924-0136(02)00103-6)
- Das A, Chatterjee S (1981) Squeeze casting of an aluminium alloy containing small amounts of SiC whiskers. *Metall Mater Technol* 137
- Delannay F, Frozen L, Peryttere A (1987) Review—the wetting of solids by molten metals and its relation to the preparation of metal-matrix composites. *J Mater Sci* 22:1
- Dieter GE (1988) Mechanical metallurgy. McGraw-Hill Higher Education, London
- Donthamsetty S, Damera NR, Jain PK (2009) Ultrasonic cavitation assisted fabrication and characterization of A356 metal matrix nanocomposite reinforced with SiC, B_4C , CNTs. *Asian Int J Sci Technol Prod Manuf Eng* 2:27–34
- Ellis M (1996) Joining of aluminium based metal matrix composites. *Int Mater Rev* 41:41–58
- Erman A, Groza J, Li X et al (2012) Nanoparticle effects in cast Mg-1 wt% SiC nano-composites. *Mater Sci Eng A* 558:39–43. doi:[10.1016/j.msea.2012.07.048](https://doi.org/10.1016/j.msea.2012.07.048)
- Esawi MK, Morsi K, Sayed A et al (2010) Effect of carbon nanotube (CNT) content on the mechanical properties of CNT-reinforced aluminium composites. *Compos Sci Technol* 70:2237–2241. doi:[10.1016/j.compscitech.2010.05.004](https://doi.org/10.1016/j.compscitech.2010.05.004)
- Evans R, Boyd J (2003) Near-interface microstructure in a SiC/Al composite. *Scr Mater* 49:59–63. doi:[10.1016/S1359-6462\(03\)00180-5](https://doi.org/10.1016/S1359-6462(03)00180-5)
- Evans A, Marchi CS, Mortensen A (2003) Metal matrix composites in industry: an introduction and a survey, vol 1. Springer, New York
- Ezatpour HR, Sajjadi SA, Sabzevar MH et al (2014) Investigation of microstructure and mechanical properties of Al6061-nanocomposite fabricated by stir casting. *Mater Des* 55:921–928
- Fecht H (1995) Nanostructure formation by mechanical attrition. *Nanostruct Mater* 6:33–42
- Fridlyander J (1994) Metal matrix composites. Springer, New York
- Friedrich HE, Mordike BL (2006) Magnesium technology: metallurgy, design data, automotive applications. Springer, Berlin
- Garcia-Hinojosa JA, Gonzalez CR, Juarez JAI, Surrapa MK (2004) Effect of grain refinement treatment on the microstructure of cast Al-7Si-SiCp composites. *Mater Sci Eng A* 386:54–60. doi:[10.1016/j.msea.2004.07.020](https://doi.org/10.1016/j.msea.2004.07.020)
- Ghomashchi M, Vikhrov A (2000) Squeeze casting: an overview. *J Mater Process Technol* 101:1–9
- Giroto FA, Quenisset JM, Naslain R (1987) Discontinuously reinforced Al metal matrix composites. *Compos Sci Technol* 30:155–184
- Goh CS, Wei J, Lee LC, Gupta M (2006) Simultaneous enhancement in strength and ductility by reinforcing magnesium with carbon nanotubes. *Mater Sci Eng A* 423:153–156. doi:[10.1016/j.msea.2005.10.071](https://doi.org/10.1016/j.msea.2005.10.071)
- Goh CS, Wei J, Lee LC, Gupta M (2008) Ductility improvement and fatigue studies in Mg-CNT nanocomposites. *Compos Sci Technol* 68:1432–1439. doi:[10.1016/j.compscitech.2007.10.057](https://doi.org/10.1016/j.compscitech.2007.10.057)
- Gu J, Zhang X, Gu M (2004) Mechanical properties and damping capacity of $(\text{SiCp}+\text{Al}_2\text{O}_3\text{-SiO}_2)/\text{Mg}$ hybrid metal matrix composite. *J Alloys Compd* 385:104–108. doi:[10.1016/j.jallcom.2004.04.106](https://doi.org/10.1016/j.jallcom.2004.04.106)
- Gu X, Zhou W, Zheng Y et al (2010) Microstructure, mechanical property, bio-corrosion and cytotoxicity evaluations of Mg/HA composites. *Mater Sci Eng C* 30:827–832. doi:[10.1016/j.msec.2010.03.016](https://doi.org/10.1016/j.msec.2010.03.016)
- Gupta M, Eugene WWL (2007) Microwaves and metals. Wiley, Hoboken

- Gupta M, Sharon NML (2011) Magnesium, magnesium alloys, and magnesium composites. Wiley, Hoboken
- Harris SJ (1988) Cast metal matrix composites. *Mater Sci Technol* 4:231
- Hassan SF, Gupta M (2005) Enhancing physical and mechanical properties of Mg using nanosized Al_2O_3 particulates as reinforcement. *Metall Mater Trans A* 36:2253–2258
- Heinrich M, Gonasagren G (2012) Semi-solid processing of alloys and composites XII. Trans Tech Publication, Durnten-Zurich
- Hong C, Kim J (2006) Development of an advanced rheocasting process and its application. In: Proceeding of the ninth international conference on the processing of semi-solid alloys and composite, Busan, Korea, pp 44–53
- Hossein-Zadeh M, Mirzaee O, Saidi P (2014) Structural and mechanical characterization of Al-based composite reinforced with heat treated Al_2O_3 particles. *Mater Des* 54:245–250. doi:[10.1016/j.matdes.2013.08.036](https://doi.org/10.1016/j.matdes.2013.08.036)
- Hu L, Wang E (2000) Fabrication and mechanical properties of SiCw/ZK51A magnesium matrix composite by two-step squeeze casting. *Mater Sci Eng A* 278:267–271. doi:[10.1016/S0921-5093\(99\)00608-5](https://doi.org/10.1016/S0921-5093(99)00608-5)
- Hu B, Peng L, Powell BR et al (2010) Interfacial and fracture behavior of short-fibers reinforced AE44 based magnesium matrix composites. *J Alloys Compd* 504:527–534. doi:[10.1016/j.jallcom.2010.05.155](https://doi.org/10.1016/j.jallcom.2010.05.155)
- Jayalakshmi S, Kailas SV, Seshan S (2002) Tensile behaviour of squeeze cast AM100 magnesium alloy and its Al_2O_3 fibre reinforced composites. *Compos Part A Appl Sci Manuf* 33:1135–1140
- Jayalakshmi S, Kailas SV, Seshan S, Fleury E (2006) Properties of squeeze cast Mg-6Zn-3Cu alloy and its saffil alumina short fibre reinforced composites. *J Mater Sci* 41:3743–3752. doi:[10.1007/s10853-005-4484-0](https://doi.org/10.1007/s10853-005-4484-0)
- Jayaramanavar P, Paramsothy M, Balaji A, Gupta M (2009) Tailoring the tensile/compressive response of magnesium alloy ZK60A using Al_2O_3 nanoparticles. *J Mater Sci* 45:1170–1178. doi:[10.1007/s10853-009-4059-6](https://doi.org/10.1007/s10853-009-4059-6)
- Kamali Ardakani MR, Khorsand S, Amirkhanlou S, Javad Nayyeri M (2014) Application of compo-casting and cross accumulative roll bonding processes for manufacturing high-strength, highly uniform and ultra-fine structured Al/SiCp nanocomposite. *Mater Sci Eng A* 592:121–127
- Kandemir S, Yalamanchili A, Atkinson H (2012) Production of aluminium matrix nanocomposite feedstock for thixoforming by an ultrasonic method. *Key Eng Mater* 504–506:339–344
- Kaufmann H, Uggowitzer P (2001) Fundamentals of the new rheocasting process for magnesium alloys. *Adv Eng Mater* 3:963
- Kennedy AR, Weston DP, Jones MI (2001) Reaction in Al–TiC metal matrix composites. *Mater Sci Eng A* 316:32–38. doi:[10.1016/S0921-5093\(01\)01228-X](https://doi.org/10.1016/S0921-5093(01)01228-X)
- Kimura Y, Mishima Y, Umekawa S, Suzuki T (1984) Compatibility between carbon fibre and binary aluminium alloys. *J Mater Sci* 19:3107
- Koli DK, Agnihotri G, Purohit R (2013) Properties and characterization of Al– Al_2O_3 composites processed by casting and powder metallurgy routes (review). *Int J Latest Trends Eng Technol* 2:486–496
- Krishnan B, Surappa M, Rohatgi P (1981) The UPAL process: a direct method of preparing cast aluminium alloy-graphite particle composites. *J Mater Sci* 16:1209
- Lee KB, Sim HS, Cho SY, Kwon H (2001) Reaction products of Al–Mg/ B_4C composite fabricated by pressureless infiltration technique. *Mater Sci Eng A* 302:227–234. doi:[10.1016/S0921-5093\(00\)01831-1](https://doi.org/10.1016/S0921-5093(00)01831-1)
- Lee KB, Sim HS, Heo SW et al (2002) Tensile properties and microstructures of Al composite reinforced with BN particles. *Compos Part A Appl Sci Manuf* 33:709–715. doi:[10.1016/S1359-835X\(02\)00011-8](https://doi.org/10.1016/S1359-835X(02)00011-8)
- Lee C, Huang J, Hsieh P (2006) Mg based nano-composites fabricated by friction stir processing. *Scr Mater* 54:1415–1420. doi:[10.1016/j.scriptamat.2005.11.056](https://doi.org/10.1016/j.scriptamat.2005.11.056)
- Li Q, Rottmair C, Singer R (2010) CNT reinforced light metal composites produced by melt stirring and by high pressure die casting. *Compos Sci Technol* 70:2242–2247

- Liao J, Tan M-J, Sridhar I (2010) Spark plasma sintered multi-wall carbon nanotube reinforced aluminum matrix composites. *Mater Des* 31:S96–S100. doi:[10.1016/j.matdes.2009.10.022](https://doi.org/10.1016/j.matdes.2009.10.022)
- Lii D-F, Huang J-L, Chang S-T (2002) The mechanical properties of AlN/Al composites manufactured by squeeze casting. *J Eur Ceram Soc* 22:253–261. doi:[10.1016/S0955-2219\(01\)00255-2](https://doi.org/10.1016/S0955-2219(01)00255-2)
- Lloyd DJ (1994) Particle reinforced aluminium and magnesium matrix composites. *Int Mater Rev* 39:1–23. doi:[10.1179/095066094790150982](https://doi.org/10.1179/095066094790150982)
- Long A, Thornhill D, Armstrong A, Watson D (2012) Predicting die life from die temperature for high pressure die casting aluminium alloy. *Appl Therm Eng* 44:100–107
- Luo ZP, Song YG, Zhang SQ (2001) A TEM study of the microstructure of SiCp/Al composite prepared by pressureless infiltration method. *Scr Mater* 45:1183–1189
- Manna A, Bhattacharayya B (2003) A study on machinability of Al/SiC-MMC. *J Mater Process Technol* 140:711–716
- Maruyama B (1998) Progress and promise in aluminium metal matrix composites. *AMPTIAC NewsLett* 2(3)
- Mazahery A, Shabani MO (2012) Mechanical properties of A356 matrix composites reinforced with nano-SiC particles. *Strength Mater* 44:686–692
- Metcalfe AG (1974) Interfaces in metal matrix composites. In: Metcalfe AG (ed) *Composite materials*. Academic, New York
- Miller W, Humphreys FJ (1991) Strengthening mechanisms in particulate metal matrix composites. *Scr Metall Mater* 25:33–38
- Miracle D (2005) Metal matrix composites—from science to technological significance. *Compos Sci Technol* 65:2526–2540
- Mortenson A, Flemmings JA, Cornie MC (1988) Solidification processing of metal matrix composites. *J Appl Meteorol* 40:12–19
- Mula S, Padhi P, Panigrahi SC et al (2009) On structure and mechanical properties of ultrasonically cast Al–2% Al₂O₃ nanocomposite. *Mater Res Bull* 44:1154–1160. doi:[10.1016/j.materresbull.2008.09.040](https://doi.org/10.1016/j.materresbull.2008.09.040)
- Naher S, Brabazon D, Looney L (2005) Development and assessment of a new quick quench stir caster design for the production of metal matrix composites. *J Mater Process Technol* 166:430–439
- Nardone V, Prewo K (1986) On the strength of discontinuous silicon carbide reinforced aluminium composites. *Scr Metall* 20:43–48
- Nguyen QB, Gupta M (2008) Increasing significantly the failure strain and work of fracture of solidification processed AZ31B using nano-Al₂O₃ particulates. *J Alloys Compd* 459:244–250. doi:[10.1016/j.jallcom.2007.05.038](https://doi.org/10.1016/j.jallcom.2007.05.038)
- Nguyen QB, Gupta M (2010) Enhancing mechanical response of AZ31B using Cu+nano-Al₂O₃ addition. *Mater Sci Eng A* 527:1411–1416. doi:[10.1016/j.msea.2009.11.002](https://doi.org/10.1016/j.msea.2009.11.002)
- Nie KB, Wang XJ, Wu K et al (2011) Processing, microstructure and mechanical properties of magnesium matrix nanocomposites fabricated by semisolid stirring assisted ultrasonic vibration. *J Alloys Compd* 509:8664–8669. doi:[10.1016/j.jallcom.2011.06.091](https://doi.org/10.1016/j.jallcom.2011.06.091)
- Noguchi T, Asano K, Hiratsuka S, Miyahara H (2008) Trends of composite casting technology and joining technology for castings in Japan. *Int J Cast Met Res* 21:219–225
- Paramsothy M, Hassan SF, Srikanth N, Gupta M (2009) Enhancing tensile/compressive response of magnesium alloy AZ31 by integrating with Al₂O₃ nanoparticles. *Mater Sci Eng A* 527:162–168. doi:[10.1016/j.msea.2009.07.054](https://doi.org/10.1016/j.msea.2009.07.054)
- Paramsothy M, Hassan SF, Srikanth N, Gupta M (2010) Simultaneous enhancement of tensile/compressive strength and ductility of magnesium alloy AZ31 using carbon nanotubes. *J Nanosci Nanotechnol* 10:956–964. doi:[10.1166/jnn.2010.1809](https://doi.org/10.1166/jnn.2010.1809)
- Reed-Hill R (1973) Role of deformation twinning in determining the mechanical properties of metals. In: *The inhomogeneity of plastic deformation*. ASM International, Materials Park
- Rohatgi PK, Asthana R, Das S (1986) Solidification, structures and properties of cast metal-ceramic particle composites. *Int Met Rev* 31:115
- Saheb N, Iqbal Z, Khalil A et al (2012) Spark plasma sintering of metals and metal matrix nanocomposites: a review. *J Nanomater* 2012:1–13. doi:[10.1155/2012/983470](https://doi.org/10.1155/2012/983470)

- Sairam K, Sonber J, Murthy T et al (2013) Influence of spark plasma sintering parameters on densification and mechanical properties of boron carbide. *Int J Refract Met Hard Mater* 42:185–192
- Saito Y, Utsunomiya H, Tsuji N, Sakai T (1999) Novel ultra-high straining process for bulk materials—development of the accumulative roll-bonding (ARB) process. *Acta Mater* 47:579–583
- Sajjadi S, Torabi Parizi M, Ezatpour H, Sedghi A (2012) Fabrication of A356 composite reinforced with micro and nano Al_2O_3 particles by a developed compocasting method and study of its properties. *J Alloys Compd* 511:226–231
- Sankaranarayanan S, Jayalakshmi S, Gupta M (2011) Effect of ball milling the hybrid reinforcements on the microstructure and mechanical properties of $\text{Mg}-(\text{Ti}+\text{n-Al}_2\text{O}_3)$ composites. *J Alloys Compd* 509:7229–7237. doi:[10.1016/j.jallcom.2011.04.083](https://doi.org/10.1016/j.jallcom.2011.04.083)
- Schultz BF, Ferguson JB, Rohatgi PK (2011) Microstructure and hardness of Al_2O_3 nanoparticle reinforced Al–Mg composites fabricated by reactive wetting and stir mixing. *Mater Sci Eng A* 530:87–97. doi:[10.1016/j.msea.2011.09.042](https://doi.org/10.1016/j.msea.2011.09.042)
- Segal V (1999) Equal channel angular extrusion: from macromechanics to structure formation. *Mater Sci Eng A* 271:322–333
- Shorowordi KM, Laoui T, Haseeb ASMA et al (2003) Microstructure and interface characteristics of B_4C , SiC and Al_2O_3 reinforced Al matrix composites: a comparative study. *J Mater Process Technol* 142:738–743. doi:[10.1016/S0924-0136\(03\)00815-X](https://doi.org/10.1016/S0924-0136(03)00815-X)
- Sklenicka V, Dvorak J, Svoboda M et al (2013) Equal-channel angular pressing and creep in ultra-fine-grained aluminium and its alloys. In: Ahmad Z (ed) *Aluminium alloys—new trends in fabrication and applications*. InTech, Rijeka
- Stacey MH (1988) Production and characterization of fibres for MMCs. *Mater Sci Technol* 4:227–230
- Su H, Gao W, Feng Z, Lu Z (2012) Processing, microstructure and tensile properties of nano-sized Al_2O_3 particle reinforced aluminum matrix composites. *Mater Des* 36:590–596. doi:[10.1016/j.matdes.2011.11.064](https://doi.org/10.1016/j.matdes.2011.11.064)
- Sun K, Shi QY, Sun YJ, Chen GQ (2012) Microstructure and mechanical property of nano-SiCp reinforced high strength Mg bulk composites produced by friction stir processing. *Mater Sci Eng A* 547:32–37. doi:[10.1016/j.msea.2012.03.071](https://doi.org/10.1016/j.msea.2012.03.071)
- Surappa M (2003) Aluminium matrix composites: challenges and opportunities. *Sadhana* 28:319
- Suryanarayana C (2001) Mechanical alloying and milling. *Prog Mater Sci* 46:1–184
- Suryanarayana C (2011) Synthesis of nanocomposites by mechanical alloying. *J Alloys Compd* 509:S229–S234. doi:[10.1016/j.jallcom.2010.09.063](https://doi.org/10.1016/j.jallcom.2010.09.063)
- Suryanarayana C, Al-Aqeeli N (2013) Mechanically alloyed nanocomposites. *Prog Mater Sci* 58:383–502. doi:[10.1016/j.pmatsci.2012.10.001](https://doi.org/10.1016/j.pmatsci.2012.10.001)
- Suslick KS, Didenko Y, Fang MM, Hyeon T, Kolbeck KJ, McNamara WB et al (1999) Acoustic cavitation and its chemical consequences. *Philos Trans R Soc Lond A* 357:335–353
- Tee KL, Lu L, Lai MO (2000) Synthesis of in situ $\text{Al}\pm\text{TiB}_2$ composites using stir cast route. *Compos Struct* 47:589–593
- Tekmen C, Ozdemir I, Cocen U, Onel K (2003) The mechanical response of Al–Si–Mg/SiCp composite: influence of porosity. *Mater Sci Eng A* 360:365–371. doi:[10.1016/S0921-5093\(03\)00461-1](https://doi.org/10.1016/S0921-5093(03)00461-1)
- Thakur SK, Balasubramanian K, Gupta M (2007a) Microwave synthesis and characterization of magnesium based composites containing nanosized SiC and hybrid $(\text{SiC}+\text{Al}[\text{sub } 2]\text{O}[\text{sub } 3])$ reinforcements. *J Eng Mater Technol* 129:194. doi:[10.1115/1.2400279](https://doi.org/10.1115/1.2400279)
- Thakur SK, Kwee GT, Gupta M (2007b) Development and characterization of magnesium composites containing nano-sized silicon carbide and carbon nanotubes as hybrid reinforcements. *J Mater Sci* 42:10040–10046. doi:[10.1007/s10853-007-2004-0](https://doi.org/10.1007/s10853-007-2004-0)
- Thakur SK, Srivatsan TS, Gupta M (2007c) Synthesis and mechanical behavior of carbon nanotube–magnesium composites hybridized with nanoparticles of alumina. *Mater Sci Eng A* 466:32–37. doi:[10.1016/j.msea.2007.02.122](https://doi.org/10.1016/j.msea.2007.02.122)

- Tjong S (2007) Novel nanoparticle-reinforced metal matrix composites with enhanced mechanical properties. *Adv Eng Mater* 9:639–652
- Tun KS, Gupta M (2009) Development of magnesium/(yttria+nickel) hybrid nanocomposites using hybrid microwave sintering: microstructure and tensile properties. *J Alloys Compd* 487:76–82. doi:[10.1016/j.jallcom.2009.07.117](https://doi.org/10.1016/j.jallcom.2009.07.117)
- Tun KS, Jayaramanavar P, Nguyen QB et al (2012) Investigation into tensile and compressive responses of Mg-ZnO composites. *Mater Sci Technol* 28:582–588. doi:[10.1179/1743284711Y.0000000108](https://doi.org/10.1179/1743284711Y.0000000108)
- Uozumi H, Kobayashi K, Nakanishi K et al (2008) Fabrication process of carbon nanotube/light metal matrix composites by squeeze casting. *Mater Sci Eng A* 495:282–287
- Vicens J, Chedru M, Chermant JL (2002) New Al–AlN composites fabricated by squeeze casting: interfacial phenomena. *Compos Part A Appl Sci Manuf* 33:1421–1423
- Wang Y, Huang J (2003) Texture analysis in hexagonal materials. *Mater Chem Phys* 81:11–26. doi:[10.1016/S0254-0584\(03\)00168-8](https://doi.org/10.1016/S0254-0584(03)00168-8)
- Wang SJ, Wu GQ, Li RH et al (2006) Microstructures and mechanical properties of 5 wt.% Al₂Yp/Mg–Li composite. *Mater Lett* 60:1863–1865. doi:[10.1016/j.matlet.2005.12.038](https://doi.org/10.1016/j.matlet.2005.12.038)
- Wang L, Turnley P, Savage G (2011) Gas content in high pressure die castings. *J Mater Process Technol* 211:1510–1515
- Wang XJ, Nie KB, Sa XJ et al (2012) Microstructure and mechanical properties of SiCp/MgZnCa composites fabricated by stir casting. *Mater Sci Eng A* 534:60–67. doi:[10.1016/j.msea.2011.11.040](https://doi.org/10.1016/j.msea.2011.11.040)
- Witkin D, Lavernia E (2006) Synthesis and mechanical behavior of nanostructured materials via cryomilling. *Prog Mater Sci* 51:1–60
- Xiong B, Xu Z, Yan Q et al (2011) Effects of SiC volume fraction and aluminum particulate size on interfacial reactions in SiC nanoparticulate reinforced aluminum matrix composites. *J Alloys Compd* 509:1187–1191. doi:[10.1016/j.jallcom.2010.09.171](https://doi.org/10.1016/j.jallcom.2010.09.171)
- Yang Y, Lan J, Li X (2004) Study on bulk aluminum matrix nano-composite fabricated by ultrasonic dispersion of nano-sized SiC particles in molten aluminum alloy. *Mater Sci Eng A* 380:378–383. doi:[10.1016/j.msea.2004.03.073](https://doi.org/10.1016/j.msea.2004.03.073)
- Yasunori M, Hiroto T, Atsushi S (1996) Method and apparatus for shaping semisolid metals. EP0745694B1
- Ye H, Liu X (2004) Review of recent studies in magnesium. *J Mater Sci* 9:6153–6171
- Ye J, He J, Schoenung J (2005) Cryomilling for the fabrication of a particulate B₄C reinforced Al nanocomposite: part I. Effects of process conditions on structure. *Metall Mater Trans A* 37(10):3099–3109
- Zhang Z, Chen D (2006) Consideration of Orowan strengthening effect in particulate-reinforced metal matrix nanocomposites: a model for predicting their yield strength. *Scr Mater* 54:1321–1326. doi:[10.1016/j.scriptamat.2005.12.017](https://doi.org/10.1016/j.scriptamat.2005.12.017)
- Zhang X, Zhang D, We R et al (1997) (SiC_w+B₄C_p)/ZK60A Mg alloy matrix composite. *Scr Mater* 37:1631–1635
- Zhang Q, Chen G, Wu G et al (2003) Property characteristics of a AlNp/Al composite fabricated by squeeze casting technology. *Mater Lett* 57:1453–1458. doi:[10.1016/S0167-577X\(02\)01006-6](https://doi.org/10.1016/S0167-577X(02)01006-6)
- Zhang Q, Ma X, Wu G (2013) Interfacial microstructure of SiCp/Al composite produced by the pressureless infiltration technique. *Ceram Int* 39:4893–4897. doi:[10.1016/j.ceramint.2012.11.082](https://doi.org/10.1016/j.ceramint.2012.11.082)
- Zheng M, Wu K, Yao C (2001) Characterization of interfacial reaction in squeeze cast SiC_w/Mg composite. *Mater Lett* 47:118–124
- Zheng MY, Wu K, Liang M et al (2004) The effect of thermal exposure on the interface and mechanical properties of Al₁₈B₄O₃₃w/AZ91 magnesium matrix composite. *Mater Sci Eng A* 372:66–74. doi:[10.1016/j.msea.2003.09.085](https://doi.org/10.1016/j.msea.2003.09.085)

Metallic Amorphous Alloy Reinforcements in Light Metal
Matrices

Jayalakshmi, S.; Gupta, M.

2015, VI, 112 p. 75 illus., 33 illus. in color., Softcover

ISBN: 978-3-319-15015-4